

LASER INTERFEROMETER GRAVITATIONAL WAVE OBSERVATORY
- LIGO -
CALIFORNIA INSTITUTE OF TECHNOLOGY
MASSACHUSETTS INSTITUTE OF TECHNOLOGY

Technical Note	LIGO-T1800447-v7
Design Requirement Document of the A+ filter cavity and relay optics for frequency dependent squeezing	
L. McCuller, L. Barsotti	

This is an internal working
note of the LIGO project.

California Institute of Technology
LIGO Project, MS 18-34
Pasadena, CA 91125
Phone (626) 395-2129
Fax (626) 304-9834
E-mail: info@ligo.caltech.edu

Massachusetts Institute of Technology
LIGO Project, Room NW17-161
Cambridge, MA 02139
Phone (617) 253-4824
Fax (617) 253-7014
E-mail: info@ligo.mit.edu

LIGO Hanford Observatory
Route 10, Mile Marker 2
Richland, WA 99352
Phone (509) 372-8106
Fax (509) 372-8137
E-mail: info@ligo.caltech.edu

LIGO Livingston Observatory
19100 LIGO Lane
Livingston, LA 70754
Phone (225) 686-3100
Fax (225) 686-7189
E-mail: info@ligo.caltech.edu

Document History

- v4 has been reviewed by Sigg et al; see review report [E1900223](#);
- v5 includes updates/corrections identified during the review
- v7 incorporates the coating design, baffle serration calculation, and an improved derivation for the phase noise requirements in sensing

Contents

1 Executive Summary	5
2 Overview	7
3 Overall performance requirement	8
4 Filter cavity linewidth requirement	8
5 Length and Finesse	8
5.1 Filter cavity loss	9
5.2 Loss per length requirement	9
6 Back-scattered light noise requirement	10
6.1 Amount of spurious interferometer light reaching the filter cavity	10
6.1.1 Interferometer readout: DC vs BHD	10
6.1.2 Faraday isolators in the squeezer path	11
6.1.3 Summary table of spurious light reaching the Filter cavity (FC)	11
6.2 Details of the scatter requirements calculation	12
6.3 Seismic isolation requirement for the filter cavity optics	12
6.4 Additional Vertical coupling on HSTS	15
6.5 Seismic isolation requirement for filter cavity relay optics	15
6.5.1 Relay optics on OPO and Output Faraday Isolator platforms (OPO Suspension (OPOS) and Output Faraday Isolator Suspension (OFIS))	16
6.5.2 Relay optics on single (HTTS) and double stage suspensions	16
6.6 Conclusions on back-scattered light noise requirements	17
7 Systems Requirements	19
7.1 Vertical Chamber placement and beam leveling	19
7.2 Vacuum pressure in the filter cavity beam tube	19
8 Filter cavity control requirements	20
8.1 RMS length noise requirement	20
8.2 Filter cavity length witness phase/length noise requirements	21
8.3 Filter cavity length control loop with 10Hz UGF	22
8.4 Filter cavity length control loop with 20Hz UGF	24
8.5 CLF Intensity Noise Requirements	24
9 Mode matching requirements	26
9.1 Active mode matching implementation	27
10 Beam size requirements	29
10.1 Filter Cavity optics	29
10.2 Relay Optics	29
10.3 Beam Tubes	30
10.4 Baffling	31

10.4.1	Scatter light level estimates	32
10.5	Specular scatterering	33
10.5.1	Baffle Implementation	34
10.6	Diffractive Baffle Scattering	34
10.6.1	Plots assuming different BRDFs of the mirrors	35
10.6.2	Derivation	39
11	Sensing Frequency Requirements	40
12	Squeezed beam alignment requirements	41
12.1	Actuators	41
12.2	Sensors	41
13	Coating Parameters	41
A	Filter cavity performance	45
A.1	Filter cavity length and loss optimization	45
A.2	Interferometer Power Dependence	45
A.3	Coating Thermal Noise Dependence	47
B	Formulas, derivations, references	48
B.1	Length Sensitivities	49
B.1.1	Length Sensitivity of a mirror	49
B.1.2	Length sensitivity, Finesse of a Fabry-Perot cavity	49
B.1.3	Length Sensitivity, Finesse of Perfectly overcoupled FP Cavity	50
B.1.4	Detuned Cavity sensitivity	50
C	Suspension and seismic models	51
C.1	HAM ISI	51
C.2	HSTS (Small Triple Suspension)	51
C.3	HTTS (Tip-Tilt Suspension)	52
C.4	Suspension point height for P2L	53
D	Details of FC length control loop	54
D.1	Length control loop with 20Hz UGF	54
D.1.1	Length control loop with 10Hz UGF	54
E	RLF phase noise derivations	57
E.1	Length Noise Requirement	57
E.2	Sensing injected length noise	58
E.3	Phase noise requirement	59
E.4	Condensed Expressions	59
E.5	Phase Noise Measurements	60
Acronyms		61

1 Executive Summary

This note summarizes the design requirements for the implementation of frequency dependent squeezing in A+.

The main conclusions that emerge from the work presented here are:

- we require a filter cavity length of 300m to obtain a 6 dB broadband squeezing enhancement (Sec. 4.5), as well as meeting the noise requirements imposed by back scattered light (Sec. 6);
- for a 300m filter cavity we require round-trip loss of 60 ppm, which are typically achievable with good quality optics (Sec. 5.1) and a Finesse $\mathcal{F} \approx 5,000$. The input coupler of the filter cavity needs to be $T_{in} \approx 1100$ ppm. For O4 power levels of 80W and the current SRM $T = 0.325$, a $T_{in} \approx 1000$ is more appropriate and will approach optimal until design power is achieved and the SRM transmissivity is lowered.
- back scattered light noise requirements impose a limit on the tolerable seismic motion not only of the filter cavity optics, but also of the relay optics that steer the squeezed beam. In particular:
 - the filter cavity optics needs to be suspended by small triple suspensions (HSTS) on HAM ISI to meet the filter cavity length noise requirements;
 - if single stage suspensions (like tip-tilt suspensions, HTTS) are used for the relay optics in the squeezed beam path, a second Faraday Isolator (SFI2) must be used in the path (on the [OPOS](#) suspension that houses the in-vacuum [Optical Parametric Oscillator \(OPO\)](#)) to meet the noise requirement; double stage suspensions, like the SAMS currently under development to house an active mode matching system ([E1800272](#)), can meet the requirements without the need of an additional Faraday (Sec. 6.5.2);
 - the current [OPOS](#) suspension hosts some of the relay optics as well, and its seismic performance meets the back scatter noise requirement only marginally below 20 Hz (without the additional Faraday); the need to move the [OPOS](#) to HAM7, with a different beam height, can be an opportunity to extend the [OPOS](#) suspension height to gain additional isolation.
- the control requirements of the filter cavity are particularly stringent. While a separate document will describe the control system in more detail, we already envision the need of two auxiliary beams to control the filter cavity, one at 532 nm to acquire lock and one at 1064 nm, frequency shifted with respect to the interferometer carrier field, to be able to control the filter cavity detuning without reintroducing excessive sensing noise (Sec. 11). Further considerations arising in [E1900223](#) also indicate:
 - the CLF power must be significantly increased from O3 levels to improve phase sensitivity. This places requirements on the CLF intensity noise, investigated in (Sec. 8.5).
 - the OPO pump light likely also has intensity noise requirements. These are difficult to compute (beyond the near term scope of this document), but must be analyzed for the final design of the locking scheme.

- Due to the backscatter and control requirements, the baseline design will include the second squeezer Faraday, SFI2, as well as double stage (SAMS) suspensions for the relay optics, with single stage tip-tilt suspensions as back-up.
- to maximize the advantage of frequency dependent squeezing, the mode matching between the [OPO](#), the filter cavity and the OMC must be as good as possible. For this reason we require an active mode matching scheme ([Active wavefront control \(AWC\)](#)) that can mode match the [OPO](#) to the filter cavity, and the filter cavity to the OMC better than the 96% level, the higher the better (Sec. 9);
- the beam sizes for a 300m cavity will easily fit on 6in suspended optics, but set aperture requirements of 2.5in from from nominal center beamline, or 5in aperture diameter if perfectly centered. The large cavity mode must then be relayed across the ISI. This is possible without clipping only if the rear surface of the cavity mirrors is curved to lens with ROC \leq 2m (Sec. 10). To relax additional layout constraints (avoiding astigmatism), the AR-side lens on the suspended optics is ideally 1m.
- backscatter noise sets a modest requirement for baffling the cavity. Only near wall scattering and specular reflections down the tube must be properly blocked. The tube should not require quadratically spaced baffles, but only a handful linearly spaced to block specular reflections. (Sec. 10.4)
- The action items of [E1900223](#) section 1.3 will be addressed in the preliminary design documents describing the ISC layout and the filter cavity control scheme.

2 Overview

One of the main components of the A+ upgrade to Advanced LIGO consists of a filter cavity (FC) to achieve broadband improvement of quantum noise via frequency dependent squeezing. Combined with a reduction of thermal noise via lower mechanical loss coating material, frequency dependent squeezing will nearly double the A+ sensitivity over Advanced LIGO (see [T1800042](#) for a description of the A+ target parameters and sensitivity). A conceptual layout of the frequency dependent squeezing implementation is shown in Fig. 1 (from [D1800027](#)). The FC will be coupled to the existing Advanced LIGO squeezed vacuum source ([D1500302](#)), and it will be integrated with the whole SQZ subsystem ([E1500359](#)).

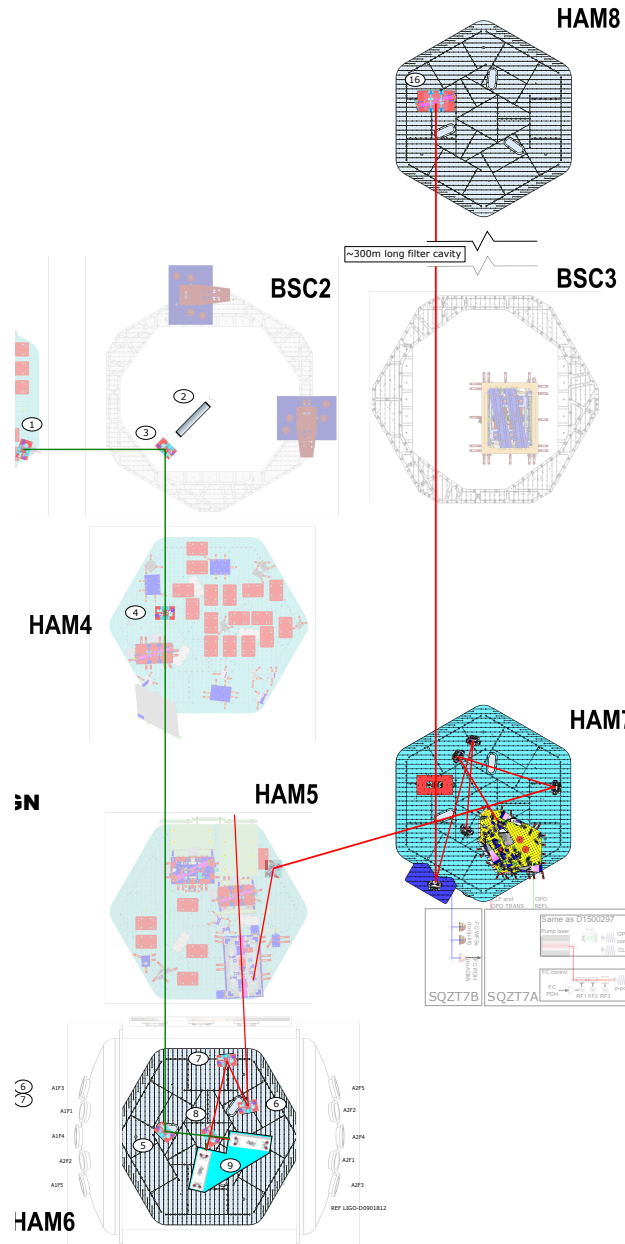


Figure 1: Conceptual layout of A+ ([D1800027](#)).

3 Overall performance requirement

The A+ target is to achieve 6 dB of broadband reduction in quantum noise via frequency dependent squeezing enhancement. In the region of the A+ noise spectrum where quantum noise is the limiting noise source, 6 dB of squeezing translates directly in a factor of 2 improvement of the noise spectrum. In other frequency regions where other noise sources like coating thermal noise are relevant, the net sensitivity improvement due to squeezing enhancement is reduced. Here we require that technical noises (back scattering noise, control noises, etc) be a factor of 10 below the target noise spectrum.

In this note we will focus on the requirements for the **FC** overall performance, optical properties and seismic isolation requirements for the **FC** optics and relay optics, as well as some of the control requirements. An additional document will describe the requirement of the active mode matching system (AWC) that will be implemented on some of the relay optics between the squeezer, the **FC** and the interferometer (**Interferometer (IFO)**), as well as in the main **IFO** readout.

4 Filter cavity linewidth requirement

To compensate for the rotation of the squeezed ellipse imposed by the **IFO** via ponderomotive squeezing [2], the **FC** half-width-half-maximum power linewidth (or cavity-pole) needs to be $2\pi \times 45$ Hz for the A+ **IFO** operating at full power with 800 kW in the arms [1]. Appendix A shows how the optimal detuning frequency changes as function of the **IFO** power.

For a low-loss optical resonator of length L and input couple transmission T_{in} , the cavity half-width-half-maximum power linewidth γ , in units of rad/s, is

$$\gamma = \frac{T_{in} + \Lambda}{2} \frac{c}{2L} \approx \frac{\pi c}{2L\mathcal{F}}, \quad (1)$$

where Λ is the round trip loss in the cavity and \mathcal{F} is the Finesse of the cavity.

A 1 km long **FC** can achieve a $\gamma = 2\pi \times 45$ Hz with a finesse $\mathcal{F} = 1500$, while a 10 m **FC** would need a finesse hundred times higher, $\mathcal{F} = 150,000$.

In other words, in order to achieve the required γ and maintain near optimal filter performance, the **FC** needs therefore to be either long (kilometer scale), or extremely high finesse.

5 Length and Finesse

There are several requirements and considerations that determine the optimal length and finesse of the **FC** for A+:

- it must satisfy the linewidth requirement (as described in section 4);
- as described in [4], for a given linewidth, the performance of the filter is determined by the loss of the **FC** per unit length. Here we follow the conservative approach that in the timescale of A+ there will not be a significant improvement in the achievable loss, and we rely on existing measurements to determine the realistic loss for a given cavity length. This leaves the length of the **FC** as parameter to adjust to achieve the desired noise performance;

- the finesse of the **FC** plays a role in the amount of back scattered light, from the **IFO** towards the **FC**, that can be tolerated. The higher the finesse, the larger is the amount of scattered light amplified by the **FC** and sent back towards the **IFO**.

Additional considerations are that:

- the cost of the **FC** increases with length, therefore we want to select the minimal length that allows to meet all of the above requirements;
- the higher the target finesse, the stricter are the loss requirements and the harder is to control the cavity. For these reasons, we want to select the minimal finesse that allows to meet all of the above requirements.

5.1 Filter cavity loss

The finesse of an optical cavity is limited by the round trip loss in the cavity Λ . Moreover, in general we want the cavity optical proprieties to be robust over variations in the loss. For an over-coupled cavity, this means that the input coupler transmission needs to satisfy $\Lambda < T_{in}$.

Although accurate modeling of loss in optical cavities based on mirror maps have been historically challenging, due to the difficulties in estimating scatter loss, several direct loss measurements on high finesse filter cavities suggest an empirical scaling law of loss versus beam size [1]. For cavities in the 5-25 m range, round trip loss of 10 ppm have been measured [3]. So, for example, a **FC** of 16 m length would need a Finesse $\mathcal{F} \approx 90,000$ to be able to achieve the required linewidth. Given the 10 ppm round trip loss, this Finesse can be achieved with an input coupler transmission $T_{in} = 60$ ppm.

For longer cavities of the order of 300 m, 60 ppm round trip loss are achievable. A **FC** of 300 m would need a Finesse $\mathcal{F} \approx 5,000$. Given the 60 ppm round trip loss, this Finesse can be achieved with an input coupler transmission $T_{in} = 1200$ ppm. Appendix A.2 shows how $T_{in} = 1100$ ppm is a better option when taking into account the **FC** performance as function of **IFO** circulating power.

5.2 Loss per length requirement

Given that for a given length, the transmission of the input coupler needs to be chosen to meet the linewidth requirement, the performance of the filter is then determined entirely by the round trip loss per unit length.

As shown in [4], 1 ppm/m is sufficient to guarantee that **Radiation Pressure Noise (RPN)** does not spoil the low frequency sensitivity in Advanced LIGO, while aiming for 6 dB of shot noise reduction. On the other hand, since A+ targets a factor of 2 reduction coating thermal noise, a lower loss per unit length is advantageous to additionally provide 6db of **RPN** reduction.

Appendix A shows the quantum noise enhancement that can be achieved for different **FC** lengths given the expected 60ppm round-trip losses, keeping all of the other baseline parameters constant. Under the assumption that the A+ coating thermal noise will be a factor of 2 lower than in Advanced LIGO (in amplitude), **we conclude that a loss per unit length of 0.2 ppm/m is a good trade-off between performance and FC length**, as

lower loss per unit length has a diminishing benefit on the A+ sensitivity. This trade-off is particularly well balanced with the requirements imposed by back-scattering, as explained in the following section.

6 Back-scattered light noise requirement

Spurious IFO light entering the squeezer port of the Output Faraday Isolator ([Output Faraday Isolator \(OFI\)](#), see [T1800398](#)) is reflected back towards the IFO by the FC and will then be following the path of the squeezed beam and be injected directly back into the IFO. Any scatter with field noise power resolvable over shot noise must be prevented. This is true also at frequencies where the IFO is limited by RPN, where the quantum noise is “amplified” by optomechanics. Due to the squeezing components located on injection side of the dark port, rather than the readout side, the phase/length noise requirements must be calculated against white quantum noise, rather than against the shaped LIGO spectrum.

The back scattered light noise depends on mainly two parameters: the amount of spurious light entering the path via the squeezed port of the OFI, and the length noise of the scattering source. This requirement imposes a limit on the tolerable length noise of the FC, as well as all of the relying optics in the path between the IFO and the FC.

The amount of spurious light entering the path depends on the type of IFO readout employed, balanced homodyne ([Balanced Homodyne Readout \(BHD\)](#)) versus DC readout, and the isolation of the OFI from its input port to its squeezer port. How much of that light reaches the FC depends also on how many additional Faraday Isolators are placed in the path.

6.1 Amount of spurious interferometer light reaching the filter cavity

Here we consider several configurations that determine the amount of spurious IFO light reaching the FC and the impact on back-scattered light requirements.

6.1.1 Interferometer readout: DC vs BHD

Advanced LIGO employs a DC readout scheme, in which DARM is intentionally detuned so as to leak some carrier field at the dark port which acts as local oscillator.

In O2, the amount of light reaching the OMC DC PDs in science mode was approximately 25 mW total. Considering up to 30% loss in the path from the OFI to the PDs, about 35 mW of IFO carrier light was entering the OFI. To account for a potentially larger DARM offset, **we use an upper limit of 50 mW entering the OFI in the DC readout case.**

A BHD scheme uses a pick-off of the IFO POP beam as local oscillator, eliminating the need for intentionally leaking some carrier field at the dark port. Due to asymmetries in the IFO arm losses, there is still some carrier that leaks through the beamsplitter. This carrier light is distinct from the “junk light” higher order modes rejected by the OMC, in that it is carried in the HG00 mode that also carries the signal and squeezing. Current measurements give the residual light level at the full design power to be between 1-7mW. **we assume 5mW of residual in-mode carrier light at design power**

Figure 2 shows a simplified layout including the relay optics between the IFO and the OPO, with a summary of the amount of spurious IFO light that enters the squeezer path.

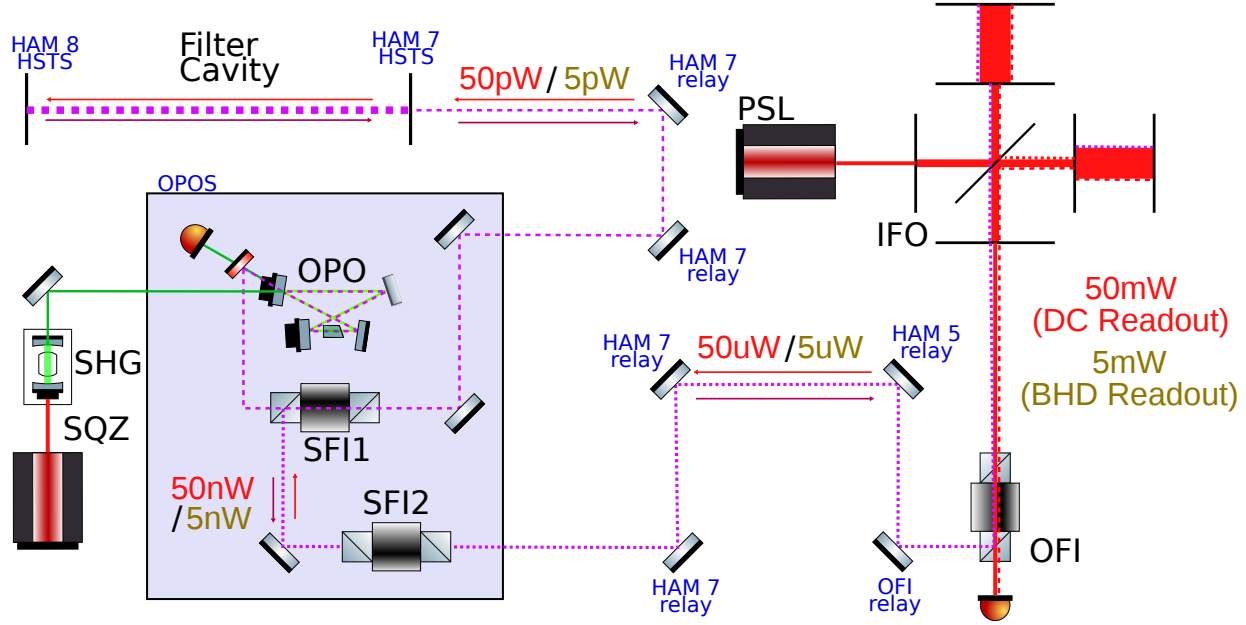


Figure 2: Simplified drawing showing the back scattered light path from the **IFO** to the **FC**. Power levels quoted here are for the Balanced Homodyne and DC readout configurations. The calculations in the following sections consider the option of having either one Faraday in the squeezed path (SFI1) or two (both SFI1 and SFI2).

6.1.2 Faraday isolators in the squeezer path

Measurements on the current Advanced LIGO **OFI** shows that the isolation from the input port of the **OFI** to the squeezer port is 25 dB (see [LLO log 24660](#)) and it strongly depends on the alignment of the **IFO** beam into the **OFI**. The new low loss **OFI** planned for A+ has a requirement of 30 dB isolation in the squeezing path ([T1800398](#)).

The SFI1 in the path has also a requirement of at least 30 dB isolation.

If an additional Faraday is placed in the path between the **IFO** and the **FC** (SFI2), we assume another 30 dB of isolation.

6.1.3 Summary table of spurious light reaching the FC

Table 1 summarizes the amount of spurious light reaching the filter cavity in the various configurations described above.

IFO configuration	OFI + SQZ.FI1 (60 dB)	OFI + SQZ.FI1 + SQZ.FI2 (90 dB)
DC readout	$50 \text{ mW} \times 10^{-6} = 50 \text{ nW}$	$50 \text{ mW} \times 10^{-9} = 50 \text{ pW}$
BHD readout	$5 \text{ mW} \times 10^{-6} = 5 \text{ nW}$	$5 \text{ mW} \times 10^{-9} = 5 \text{ pW}$

Table 1: Amount of spurious **IFO** light reaching the **FC** in various configurations, driving the requirements of the length noise of the **FC**.

6.2 Details of the scatter requirements calculation

In the following sections we are going to calculate the requirement imposed by back scattered light noise on the length noise $N(f)$ of various components (**FC** optics, relay optics).

By following the same approach as in [P1200155](#), we derive expressions which link the length noise of the various components to back scattered light noise, and we require the back scattered light noise to be small compared to the **IFO** total noise.

Details of the expressions presented in the next sections can be found in Appendix [B](#).

We consider the following safety margins and factors:

- $C_{\text{safe}} = 1/10$: imposing the back scattered noise to be a factor of 10 below the total **IFO** (unsqueezed) noise;
- $C_{\text{sqz}} \approx \frac{1}{2}$: additional factor that explicitly takes into account the fact that any amount of squeezing enhancement further reduce the amount of tolerable back scattered light. Instead of using a broadband factor of $C_{\text{sqz}} = 1/2$, consistent with the squeezing broadband enhancement of 6 dB, we relax the requirement by considering that other (non-quantum) noises limit the **IFO** sensitivity. C_{sqz} becomes therefore a frequency dependent parameter, as shown in Fig. 3, with $C_{\text{sqz}} = 1/2$ only at those frequency where the **IFO** is dominated by quantum noise and the other noises are negligible.
- pre/post Faraday relay optics : The calculation does not depend on the placement with respect to the Faraday Isolators. Relay optics earlier in the chain have a larger carrier to generate noise sidebands, but the sidebands are then attenuated by the isolators.
- Multiplicity: These plots **do not account for the multiplicity of the relay optics or **FC** optics** This is partially since noise for a given ISI will be have coherence between suspensions and can potentially cancel or add for a given layout geometry.
- Double pass: These plots do account for the forward and reverse passes across relay optics. The **FC** detuning rotates the carrier 90 degrees between these passes, so the sensitivity enhancement is $\sqrt{2}$ rather than full 2 from the coherent addition of the passes.

6.3 Seismic isolation requirement for the filter cavity optics

Here we calculate the requirement for the length noise of the **FC** as function of frequency, $N_{\text{FC}}(f)$. The sensitivity formula Eq. 82 of Sec. [B.1.3](#), as well as the transfer function of the detuned cavity (Eq.), give the field generated by length noise in the **FC**. The modulated field scales with the input light level, giving a sensitivity which depends on the total isolation.

By using the levels of scattered light power incident on the **FC** as described in table [1](#), we derive the following requirements for each scenario:

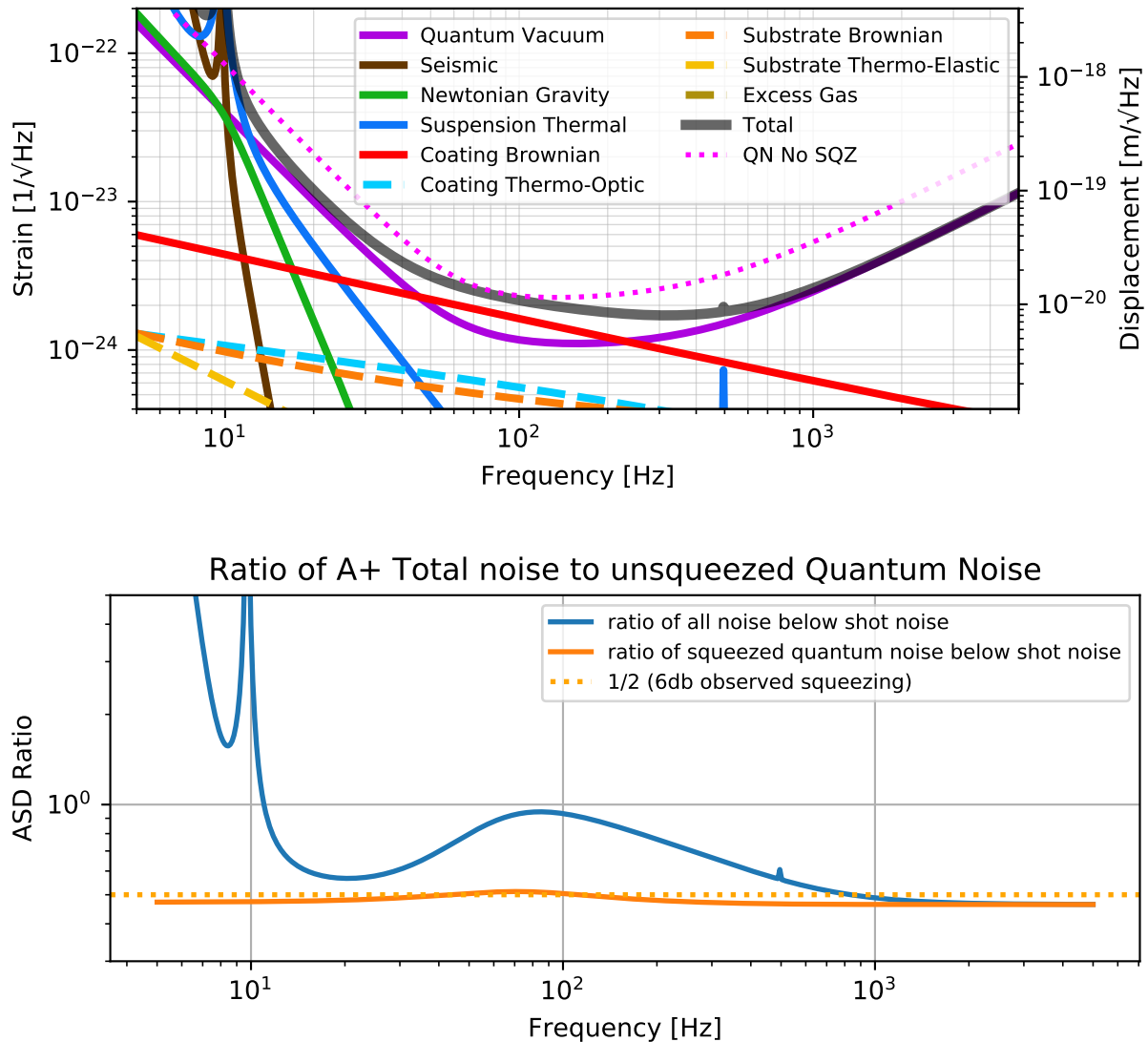


Figure 3: The upper plot shows the A+ design sensitivity curve with the main fundamental noises, as well as the unsqueezed quantum noise curve. The lower plot shows the C_{sqz} factor used in the length noise requirements. It is calculated by taking the ratio of all of the A+ fundamental noises and (unsqueezed) shot noise. This factor represents the additional safety margin needed when quantum noise is reduced by squeezing, therefore making the back scattered light noise requirement more stringent.

$$N_{FC}(f) \leq C_{\text{safe}} C_{\text{sqz}} \frac{Q_\lambda}{|\vec{H}_{FC\Delta L}(f_\Omega)|} \quad (2)$$

$$\leq 3.3 \cdot 10^{-18} \frac{\text{m}}{\sqrt{\text{Hz}}} \left(\frac{P_{\text{leak}}}{50\text{nW}} \right)^{-1/2} \left(\frac{L_{\text{FC}}}{300\text{m}} \right) \left(\frac{f_{\text{FC}}}{50\text{Hz}} \right) \quad (3)$$

$$\leq 1.0 \cdot 10^{-17} \frac{\text{m}}{\sqrt{\text{Hz}}} \left(\frac{P_{\text{leak}}}{5\text{nW}} \right)^{-1/2} \left(\frac{L_{\text{FC}}}{300\text{m}} \right) \left(\frac{f_{\text{FC}}}{50\text{Hz}} \right) \quad (4)$$

$$\leq 1.0 \cdot 10^{-16} \frac{\text{m}}{\sqrt{\text{Hz}}} \left(\frac{P_{\text{leak}}}{50\text{pW}} \right)^{-1/2} \left(\frac{L_{\text{FC}}}{300\text{m}} \right) \left(\frac{f_{\text{FC}}}{50\text{Hz}} \right) \quad (5)$$

$$\leq 3.3 \cdot 10^{-16} \frac{\text{m}}{\sqrt{\text{Hz}}} \left(\frac{P_{\text{leak}}}{5\text{pW}} \right)^{-1/2} \left(\frac{L_{\text{FC}}}{300\text{m}} \right) \left(\frac{f_{\text{FC}}}{50\text{Hz}} \right) \quad (6)$$

Fig. 4 shows the **FC** longitudinal noise calculated by considering a linear 300 m **FC** with **Small triple suspension (HSTS)**, overlaid with requirements. The **HSTS** suspensions are placed on a standard aLIGO HAM ISI, whose performance is described in [T1800066](#), and calculated as detailed in Appendices [C.4](#) and [C](#).

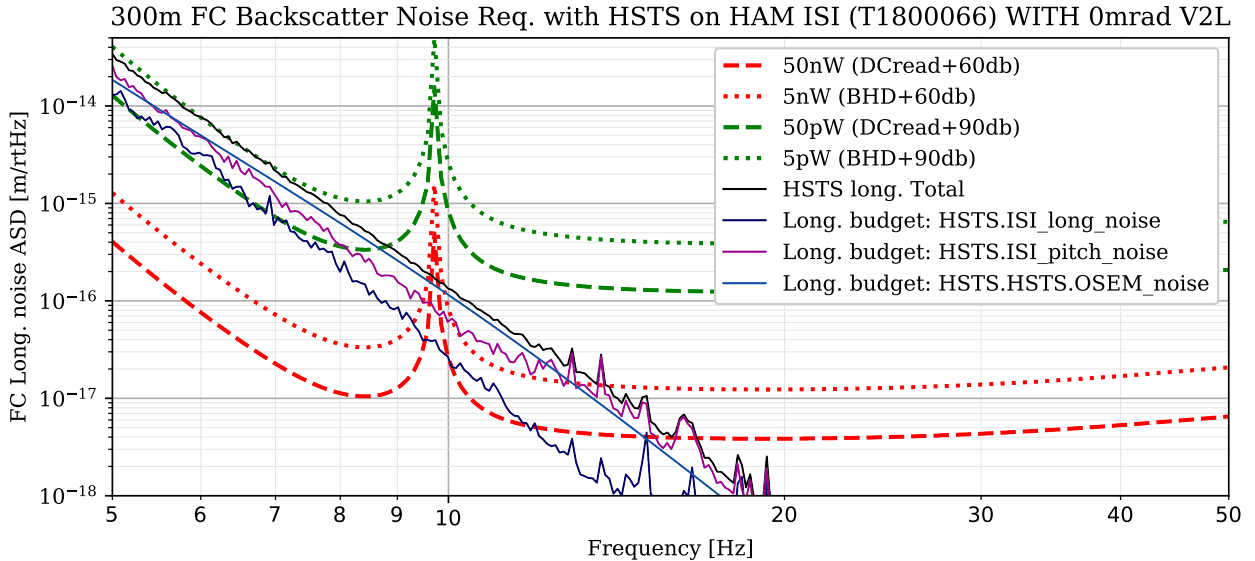


Figure 4: Length noise of a 300m **FC** with **HSTS** on standard aLIGO HAM ISIs ([T1800066](#)), compared to length noise requirement imposed by back scattered light noise.

We can extract the following conclusions:

- if we include a second Faraday on the VOPO suspension (SFI2 on the **OPOS**, see Fig. 2), the **FC** length noise is a factor of 10 or more below requirements for both **BHD** and DC configurations (reminder: the requirement does already include a factor of 10 safety margin);
- in the scenario in which we use **BHD** readout without a second Faraday, the total length noise of the **FC** meets the requirement above 15 Hz, while it is at the requirement level between 10 - 15 Hz;

- in the scenario in which we use DC readout without a second Faraday, the total length noise of the FC is a factor of 3 - 5 above requirement below 15 Hz.

In summary, **HSTS small triple suspensions on an HAM ISI table** meet the back scatter noise requirements above 15 Hz for all of the scenarios considered here, including the most demanding case of DC readout without the presence of an additional Faraday in the squeezing path. Given that the requirements already include a factor of 10 safe margin, the **HSTS** on HAM ISI is also acceptable below 15 Hz.

Note that this calculation is done open loop. The impact of a length control loop is studied in Sec. 11.

6.4 Additional Vertical coupling on HSTS

Using the same model and noise sources of the previous section, but including an additional 3 mrad of coupling of the mirror vertical motion into length is shown in Fig. 5. This plots shows that the bounce mode approaches the limiting noise floor only for the largest level of backscattered light considered. With some additional damping of bounce modes, even that level of backscatter could be accommodated with this additional vertical coupling,

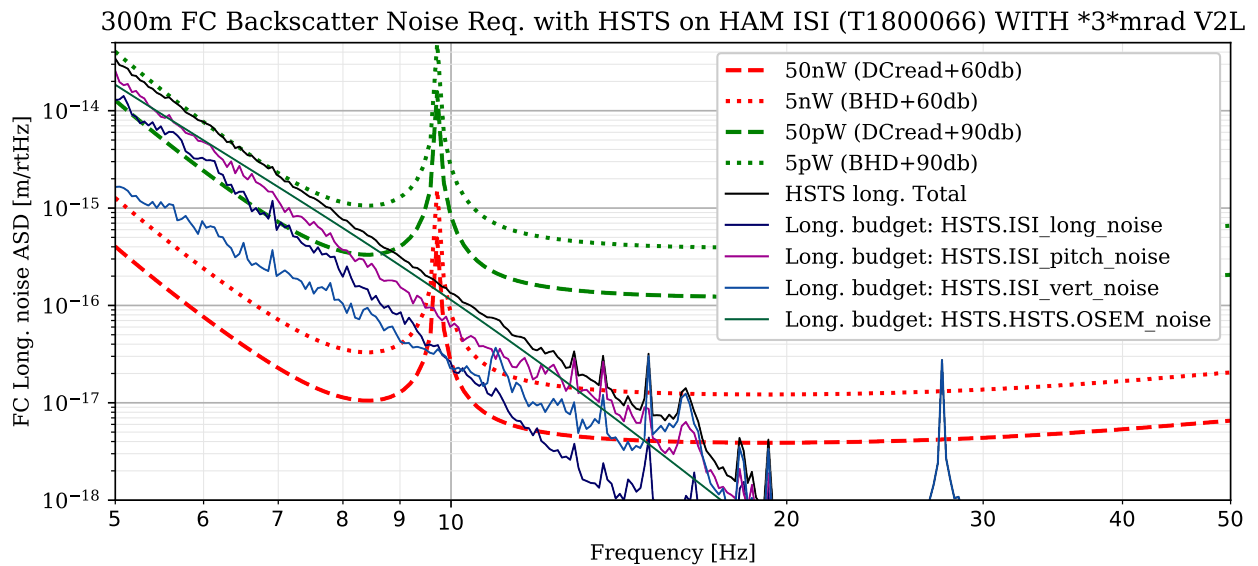


Figure 5: Length noise of a 300m **FC** with **HSTS** on standard aLIGO HAM ISIs ([T1800066](#)), with 3 mrad of vertical to length coupling, compared to length noise requirement imposed by back scattered light noise.

6.5 Seismic isolation requirement for filter cavity relay optics

There are several relay optics that carry the squeezed beam to the **IFO** and they are distributed across multiple types of suspensions.

Here we calculate the length noise requirements for the various back scattered light levels reported in table 1 and compare them with the length noise for various types of suspensions in the path.

Using eq. 70 and the levels of scattered light power incident on the FC as described in table 1, we derive the following requirements for each scenario:

$$N_{aux}(F) \leq C_{\text{safe}} C_{\text{sqz}} C_{2\text{pass}} \frac{Q_\lambda}{\delta_{\Delta L}^{e_{\text{mirror}}}} \quad (7)$$

$$\leq 4.1 \cdot 10^{-15} \frac{\text{m}}{\sqrt{\text{Hz}}} \left(\frac{P_{\text{leak}}}{50\text{nW}} \right)^{-1/2} \leq 1.3 \cdot 10^{-14} \frac{\text{m}}{\sqrt{\text{Hz}}} \left(\frac{P_{\text{leak}}}{5\text{nW}} \right)^{-1/2} \quad (8)$$

$$\leq 1.3 \cdot 10^{-13} \frac{\text{m}}{\sqrt{\text{Hz}}} \left(\frac{P_{\text{leak}}}{50\text{pW}} \right)^{-1/2} \leq 4.1 \cdot 10^{-13} \frac{\text{m}}{\sqrt{\text{Hz}}} \left(\frac{P_{\text{leak}}}{5\text{pW}} \right)^{-1/2} \quad (9)$$

The requirements have been computed by taking into account the following aspects:

Adjustment for double pass: the backscatter beam on the relay optics will pass the optics twice, once one the way to the FC, and once following the SQZ beam to the IFO. The FC is detuned by one cavity pole, and so the carrier quadrature is 90deg out of phase on the second pass from the first pass. For this reason, the factor $C_{2\text{pass}} = \frac{1}{\sqrt{2}}$ also modifies the safe limit;

Adjustment for multiplicity: these safe limits are not adjusted for the sheer number of suspended optics (6). This factor is important because some noise will add in quadrature, but some will also add coherently amongst these suspensions, so the marginal meeting of the safe limit by the [Tip-tilt suspension \(HTTS\)](#) for the DC readout with 60db of isolation is likely not sufficient.

Some additional details about the calculation related to the propagation of the seismic noise through the various suspensions can be found in Appendix [C.4](#).

6.5.1 Relay optics on OPO and Output Faraday Isolator platforms (OPOS and OFIS)

The SFI1 and SFI2 isolators will relay the beam between [OPO](#), [FC](#), and [OFI](#) and are all mounted on the suspended [OPO](#) platform, [OPOS](#). These are single suspensions and can add phase noise to the backscattered light. For the [OPOS](#), this can be mitigated somewhat by adjusting the input and output angles to have an effectively large angle of incidence. The noise performance of the [OPOS](#) is shown in Fig. 6

For injection into the [OFI](#), the last relay optic is on the [OFIS](#) and the PBS to insert the beam is also a relay optic. Only the [OPOS](#) is plotted here. The drawing [D0900136](#) shows that the [OFIS](#) uses a substantially longer suspension length than the [OPOS](#), and the noise floor of the [OFIS](#) should go as the ratio of the suspension lengths of the [OFIS](#) and the [OPOS](#).

Based on Fig. 6, we conclude that the back scattered noise due to the relay optics on the [OPOS](#) platform is not a limiting noise source in all cases, except for the DC readout configuration with only one Faraday on the [OPOS](#) (DC readout + 60 dB isolation). In that case, the safe requirements are not met below 20 Hz.

6.5.2 Relay optics on single (HTTS) and double stage suspensions

Most of the relay optics in between [OPO](#), [FC](#), and [OFI](#) will be 2" optics suspended and equipped with [AWC](#). Here we calculate the length noise for a typical aLIGO, [HTTS](#) on HAM

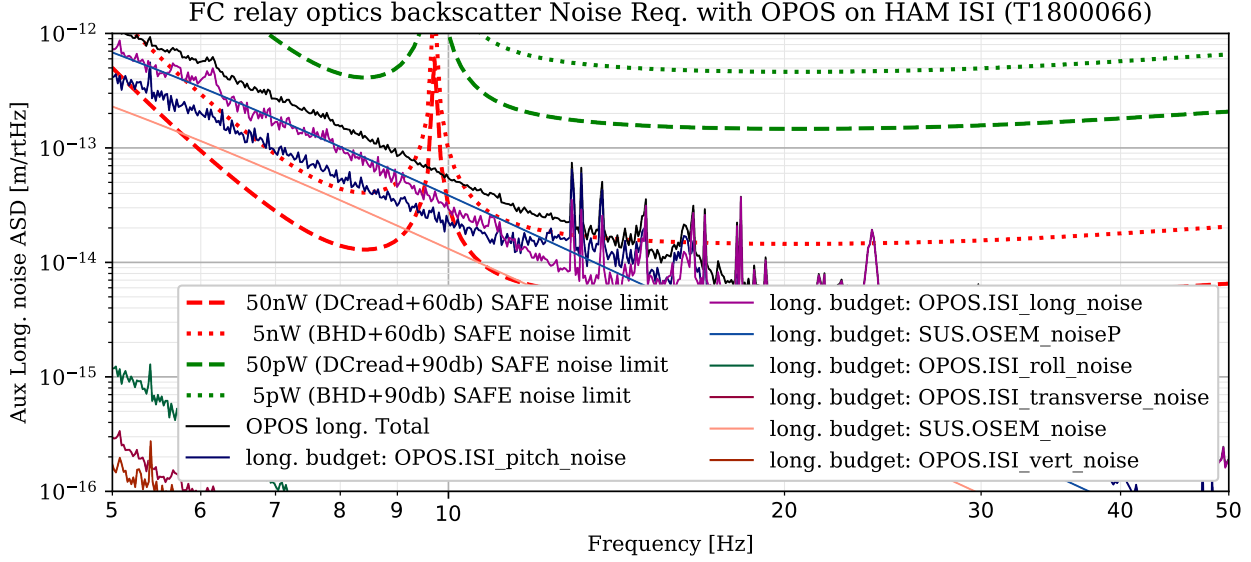


Figure 6: Length noise of an [OPOS](#) suspension on standard aLIGO HAM ISIs ([T1800066](#)), compared to length noise requirement imposed by back scattered light noise.

ISI, as well as for a double stage suspension. While a dedicated single stage suspension for a 2" optics is under design ([E1800272](#)), here we consider the two stage OMC suspension (OMCS) as example.

Fig. 7 compares the [HTTS](#) length noise with the requirements imposed by back scattered light. We can see that below 20 Hz, single stage tip-tilt suspensions do not meet the requirements if only one Faraday is placed on the [OPOS](#), especially considering that up to 6 of these suspensions will be used in the path. The addition of a Faraday (and therefore a 90dB isolation total) ensures that the tip-tilt is compatible with requirements.

Fig. 8 shows the same plot for a two stage suspension (OMCS as example). In this case the noise requirements are largely met for all of the configurations, therefore not requiring the addition of a second Faraday on the [OPOS](#), as well as being compatible with multiple suspensions used in the path.

6.6 Conclusions on back-scattered light noise requirements

- In O4 we plan to maintain DC readout, while deploying frequency dependent squeezing. Given the analysis described in this section, the conclusion is that we need the second squeezer Faraday SFI2 to comfortably meet the noise requirements down to 10 Hz. Once [BHD](#) is operational, we might have the option to remove SFI2.
- With SFI2 in the squeezer path, we have the option of using single-stage tip-tilt suspensions for the relay optics. However, given that double-stage SAMS suspensions are going to be needed anyway for the optics with AWC, it would be optimal to use SAMS suspensions for all of the relay optics.

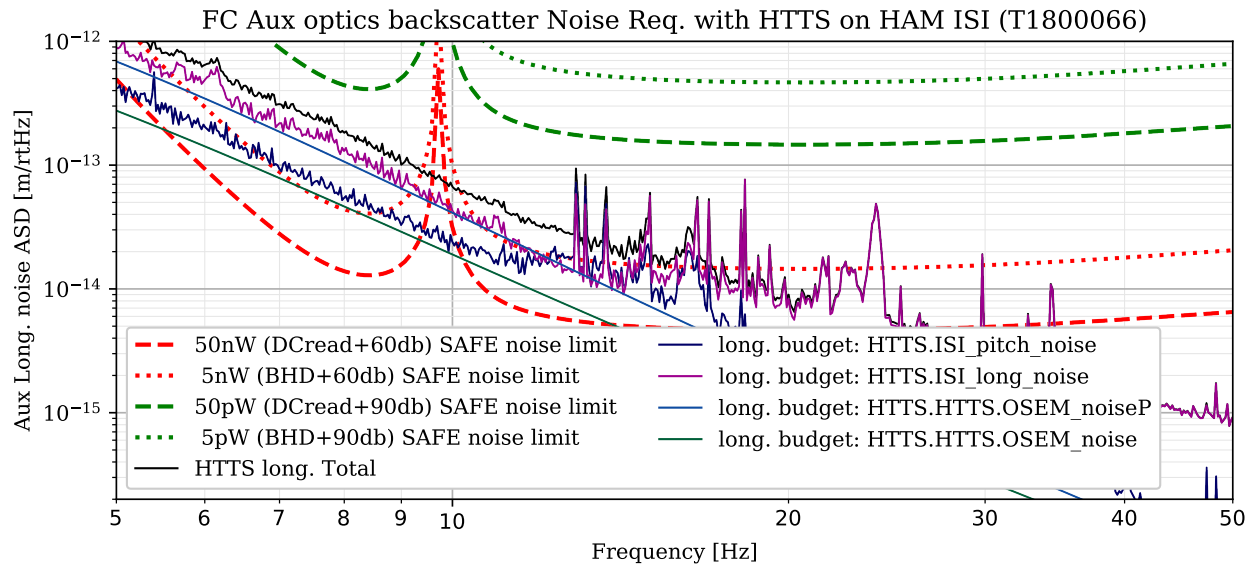


Figure 7: Length noise of an HTTS (single stage, tip-tilt) suspension on standard aLIGO HAM ISIs (T1800066), compared to length noise requirement imposed by back scattered light noise.

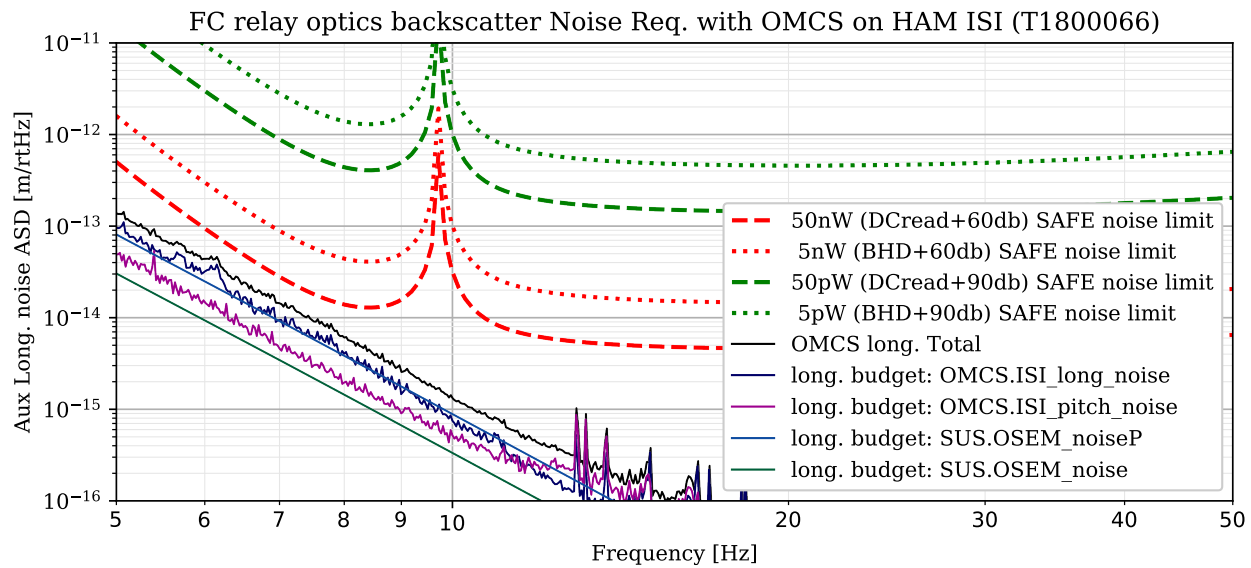


Figure 8: Length noise of an OMCS type suspension (double stage) on standard aLIGO HAM ISIs (T1800066), compared to length noise requirement imposed by back scattered light noise. A dedicated double stage suspension for a single 2" optic is under design (E1800272), so here we use the transfer functions of the OMCS as example.

7 Systems Requirements

This section frames the low level requirements from backscatter and optical performance to constraints known to be relevant for systems and civil engineering.

7.1 Vertical Chamber placement and beam leveling

In the event that the chambers hosting the filter cavity suspensions must be placed at different heights, the only known issue arises from vertical to length noise coupling in the triple suspensions used for the cavity optics. Assuming a 3 mrad inclination angle, the noise in this arrangement is plotted in Fig. 5, showing that it does not significantly contribute to the overall length noise. Further confirmation of this noise analysis, based on past noise studies of the HSTS, is provided by Norna Robertson in [T1800484](#).

7.2 Vacuum pressure in the filter cavity beam tube

The LIGO Vacuum Team has compared the performance of the envisioned vacuum system for the filter cavity beam tube with requirements (see [E1800327](#) for the full analysis).

Requirements have been set such that the displacement noise induced by fluctuations in the effective refractive index of residual gas in the beam tube is at least 1/3 of the most stringent length noise requirement imposed by back scatter calculation (keeping in mind that there is already a factor of 10 safety margin in the back scatter noise requirement).

We therefore use Eq. 3 in Sec. 6.3 as the most stringent length noise requirements (with 50 nW of spurious light reaching the filter cavity), and we impose another factor of 1/3 on top of that, yielding a length noise requirement of $2.2 \cdot 10^{-18} \frac{\text{m}}{\sqrt{\text{Hz}}}$.

The conclusion, summarized in Mike Zucker's plot reported here in Fig. 9, is that the baseline vacuum system designed for the filter cavity beam tube (see [LIGO-D1800238](#)) largely meets the requirements with another factor of 40 safety margin.

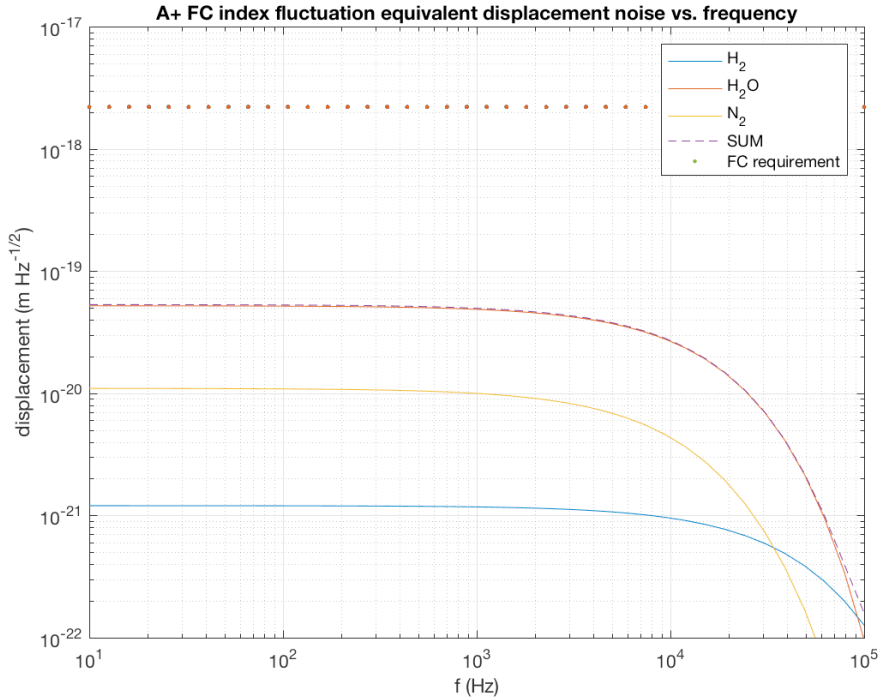


Figure 9: Displacement noise caused by fluctuations in the effective refractive index of residual gas in the filter cavity beam tube compared with requirements.

8 Filter cavity control requirements

Two main requirements must drive the design of the **FC** control scheme:

- the RMS of the **FC** length noise, that becomes frequency dependent phase noise of the **FC** due to length noise conversion into phase fluctuations;
- the back scattered light noise requirement, as the sensing noise reintroduced by the control loop which keeps the **FC** on its operating point contributes to the length noise of the **FC**.

The first requirement favors a **FC** length control loop with high bandwidth, so as to minimize the length noise RMS, while the second requirement favors a low bandwidth loop to minimize the sensing noise reintroduced into the loop that becomes length noise.

8.1 RMS length noise requirement

The requirement on the RMS of the **FC** length noise is due to the fact that the length noise is converted into phase fluctuations, becoming frequency dependent phase noise. Since the cavity is detuned and the squeezing phase itself is a function of frequency, an exact expression for the frequency dependent effect of phase fluctuations is involved to calculate, but ultimately scales with the general phase sensitivity of a Fabry Perot cavity. The frequency dependence of the phase noise, below $T(f_\Omega)$, peaks at the detuning frequency, where the

sideband phase is rotating the strongest, around 50 Hz.

$$\text{PSD}[Q; f_\Omega] = 10^{-\text{dB}_{\text{sqz}}/10} + 10^{+\text{dB}_{\text{asqz}}/10} \text{VAR}[\delta l] \left(\frac{2c}{\lambda f_p L_{\text{FC}}} \right)^2 T(f_\Omega) \quad (10)$$

$$\text{VAR}[\delta l] = \text{RMS}[\delta l]^2 = \int \text{PSD}[\delta l; f] df \quad (11)$$

Where $\text{PSD}[Q; f_\Omega]$ is the power spectral density relative to the standard quantum limit, with the **FC** and squeezer achieving an observed dBsqz level of quantum noise reduction, while producing dBAsqz of antisqueezing. For A+ the observed squeezing level will be 6db and the generated antisqueezing level should be 12db.

The total variance of the **FC** length is given by $\text{VAR}[\delta l]$, and this is assumed to be dominated by noise at frequencies small compared to the 50 Hz cavity pole. Given this assumption, the frequency dependence of the phase noise is

$$T(f_\Omega) = \frac{f_{\text{SQL}}^4}{f_{\text{SQL}}^4 + f_\Omega^4} \left(\frac{f_p^4}{2(f_p^2 + (f_\Omega + f_{\text{det}})^2)^2} + \frac{f_p^4}{2(f_p^2 + (f_\Omega - f_{\text{det}})^2)^2} \right) \quad (12)$$

The derivation of this expression is involved, but the models given in fig. 14 using the code developed for [1] treat the length noise as a perturbation of the detuning frequency and confirm this phase noise analysis.

For the squeezing degradation to be minimal at all frequencies, the RMS length noise of the **FC** must be such that the antisqueezing only injects as much noise as the squeezed shot-noise itself. This actually corresponds to a reduction from 6db of broadband squeezing to 3db near 50Hz if this limit is saturated, so the total variance of the noise additionally has the safety margin factor of 10 applied.

$$\text{RMS}[\delta l]_{\text{safe}} < \sqrt{C_{\text{safe}}} 10^{-(\text{dB}_{\text{sqz}} + \text{dB}_{\text{asqz}})/20} \frac{\lambda f_p L_{\text{FC}}}{2c} = 8 \cdot 10^{-13} \text{m} \quad (13)$$

which corresponds to 30mRad of phase noise at the detuning frequency. This level is similar to what is easily achievable for the broadband phase noise. Ignoring the safety margin gives a residual length noise requirement of

$$\text{RMS}[\delta l]_{\text{marginal}} < 2.5 \cdot 10^{-12} \text{m} \quad (14)$$

Secs. 8.3 and 8.4 show that this is achievable for the current ISI noise and **HSTS** performance with a loop bandwidth between 10Hz and 20Hz.

8.2 Filter cavity length witness phase/length noise requirements

The principle difficulty with controlling the **FC** length is that the length sensing signal for the **FC** must be delivered with a frequency shifted beam. This is to avoid reintroducing noise at the IFO carrier frequency. This frequency shifted beam will be generated with a VCO that has frequency noise. This frequency noise is a sensing noise for the signal which

the loop will convert into length noise. The requirements for this phase noise are derived in App. E, but can be related to the existing length noise requirements using the conversion:

$$\frac{\delta f}{f_\lambda} = \frac{\delta l_{\text{FC}}}{L_{\text{FC}}} \quad (15)$$

converted to a requirement

$$\delta l_{\text{FC}} = \frac{\lambda L_{\text{FC}}}{c} \delta f \quad (16)$$

Using the values for the aLIGO VCO's and Wenzel OXCO 78MHz oscillators from the [awiki RfDesign](#) page measures a phase noise of $1 \cdot 10^{-6}$ at 100Hz, which falls as $1/f$ in the ASD (actually slightly less for the Wenzel OXCO, but $1/f$ is typical for VCOs). This gives a white frequency noise of $1 \cdot 10^{-4} \frac{\text{Hz}}{\sqrt{\text{Hz}}}$. The sensing noise for such a VCO generated sensing signal is $1 \cdot 10^{-16} \frac{\text{m}}{\sqrt{\text{Hz}}}$.

This noise level is larger than the safe noise limit for 60db worth of Faraday isolators (2, rather than 3) in either the DC readout of [BHD](#) cases. See figures 11 and 12. Since it is a sensing noise, it may be avoided partially using a low bandwidth loop. The existing AOMs used to generate the CLF may be used to generate a new field that is resonant or near resonant in the filter cavity to allow sensing. The phase locking scheme of any new fields must ensure that the frequency sources can be reduced to the required level. The 10Hz control loop analyzed in the following section imposes the frequency and phase noise requirements on the sensing field of Fig. 10.

While such a scheme provides a means to avoid this fundamental sensing noise, path length phase noise in the transport of the sensing field will also generate a phase noise which the control system will inject. The “effective” phase noise of the existing backscatter requirements on the relay length noise are:

$$\delta\theta_{\text{path}} < \frac{4\pi}{1064\text{nm}} 1.3 \cdot 10^{-13} \frac{\text{m}}{\sqrt{\text{Hz}}} \left(\frac{P_{\text{leak}}}{50\text{pW}} \right)^{-1/2} \quad (17)$$

$$< 1.5 \cdot 10^{-6} \frac{\text{rad}}{\sqrt{\text{Hz}}} \quad (18)$$

Which gives that the displacement noise requirements on the relays are not increased due to the controls sensing of the filter cavity optics.

Historically, this sensing field has been done with a 532nm beam in the 2m as well as the 16m [FC](#) experiments at MIT [5]. However, the above requirement is hard to meet with a 532nm beam, as the sensing noise is too high. For this reason, as shown in the A+ frequency dependent squeezing conceptual layout [E1800023](#), we plan to use a 532nm beam for acquiring the lock of the filter cavity, and a 1064nm frequency shifted beam, phase locked to the main [IFO](#) beam, to control the [FC](#) detuning.

8.3 Filter cavity length control loop with 10Hz UGF

The ISI and [HSTS](#) noise models are used to model the residual RMS in a realistic control loop. Appendix D shows the details of the filters used. This loop includes boosts to whiten

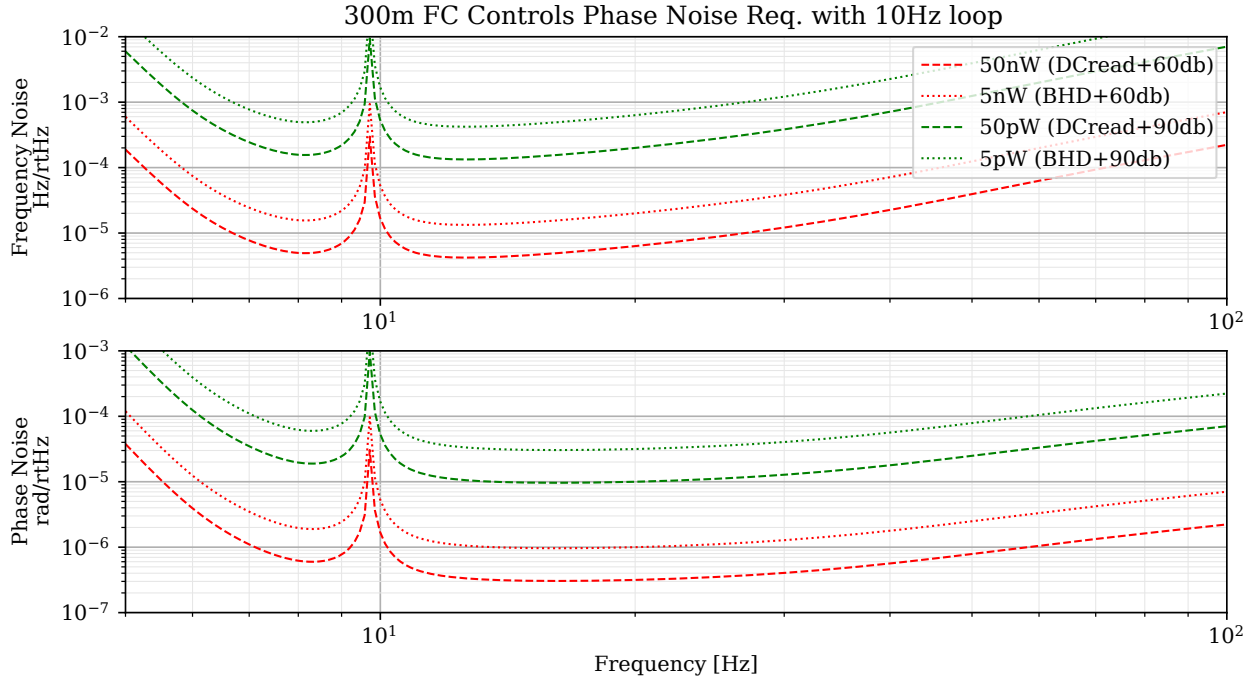


Figure 10: The phase noise requirements inferred from sensing noise injection of a 10Hz control and the length noise requirements for DC/BHD readout with one or two Faradays in the squeezing path (60dB/90dB isolation, including one pass in the OFI). For O4 (frequency dependent squeezing with DC readout) the relevant curve is "DCread + 90 dB".

the ground noise as well as resonant gains (pole zero pairs) to compensate for the damped suspension Q. In practice, those resonant gains would be naturally present in the actuator response. This loop does not include strong rolloff above the UGF, which may need revision depending on actuator RMS voltage requirements.

The loop doesn't include great phase margin at the UGF, with only about 30deg. This small margin and the weak antiboost near the UGF, causes mild gain peaking in the closed loop gain, and considerable sensing noise injection $\frac{G}{1-G}$ below the UGF, but it is only $\sqrt{2}$ at 10Hz.

Figure 33 Shows the residual noise as well as the cumulative RMS, which is not dominated by any particular peaks due to the loop resgains. The total residual length noise for this loop only achieves the marginal RMS requirements. This is because the high resonance of the HSTS occurs around 3Hz, which is also where the zeros of the boosts need to be located to achieve acceptable phase margin. With the $1/F^3$ loop within boosts, the RMS roughly scales inversely as the cube of the UGF.

Figure 11 then shows that the loop gain peaking does not strongly enhance the ground spectrum to violate the safety margins, but the length noise will clearly be dominated by VCO sensing noise even with a Wenzel OXCO baseline.

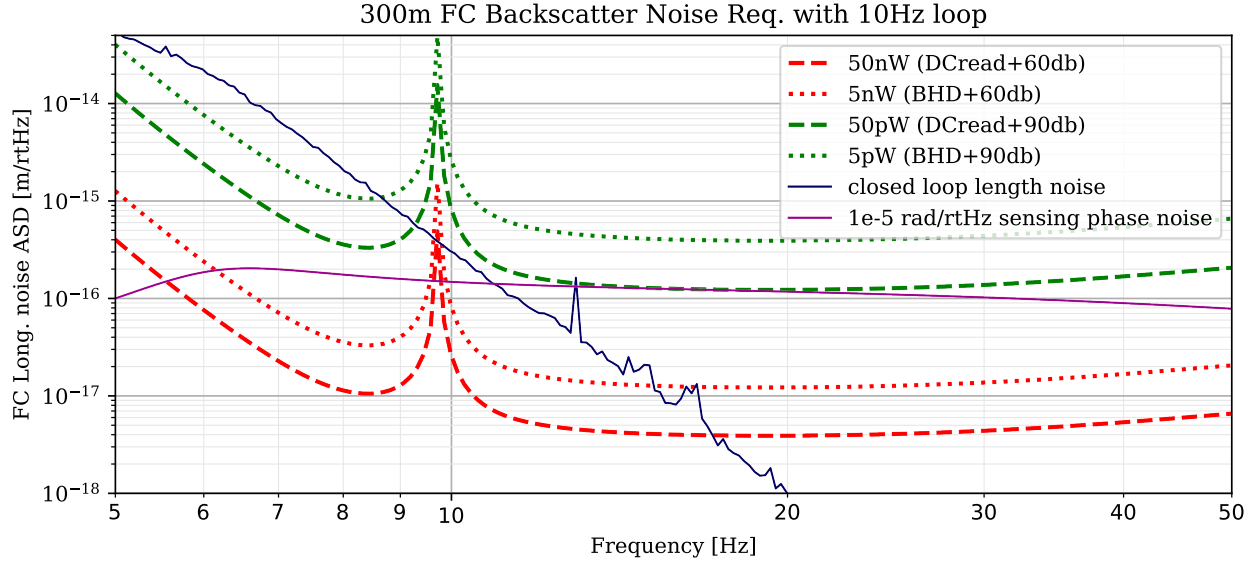


Figure 11: Using a 10Hz loop, these are the ground noise with gain peaking included, as well as the loop injection of VCO-limited sensing noise.

8.4 Filter cavity length control loop with 20Hz UGF

This model is only a minimal modification of the 10Hz version, scaling the boost zeros with the UGF to get the cubic reduction in RMS. Appendix D shows the details of the filters used. Figure 31 gives the RMS, which meets the safe phase noise requirement, but is somewhat less favorable for the safe limit of length noise. The sensing noise is considerably worse for this loop due to putting the gain peaking into the GW band.

and Figure 12.

In the case where the VCO noise is considerably reduced below the Wenzel, the sensing noise becomes irrelevant and ideal loop would be 20-50Hz, where the HSTS noise is so low that gain peaking is irrelevant, and the ground noise at 10Hz may be reduced by the loop as well.

8.5 CLF Intensity Noise Requirements

With this phase noise requirement, the laser must be stabilized using some reference. The SQZANGLE loop stabilizes the squeezer laser to the interferometer phase at the AS port. The interferometer phase has been stabilized by the common mode servos, and at 10 Hz, should reflect the phase noise residual of the common mode servo. The length noise of the interferometer only amounts to $1 \cdot 10^{-6} \frac{\text{Hz}}{\sqrt{\text{Hz}}}$.

In that case, the sensing noises of the CLF optical signal should limit the phase noise. The power level of the CLF sets the quantum limited sensitivity to phase. With 2uW of CLF incident on the OMC, and 1% transmission through, there is 20nW on the OMCPDs. For a single-sideband heterodyne detection, this gives a phase sensitivity of $\frac{2Q_\lambda}{\sqrt{10nW}} = 3 \cdot 10^{-6} \frac{\text{rad}}{\sqrt{\text{Hz}}}$.

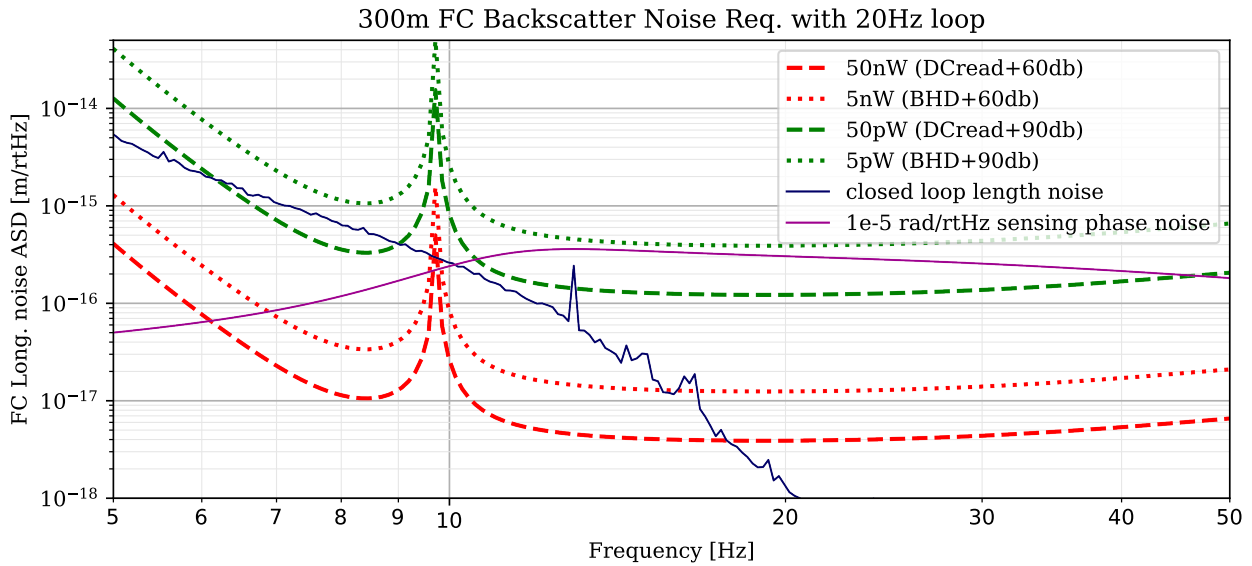


Figure 12: Using a 10Hz loop, these are the ground noise with gain peaking included, as well as the loop injection of VCO-limited sensing noise.

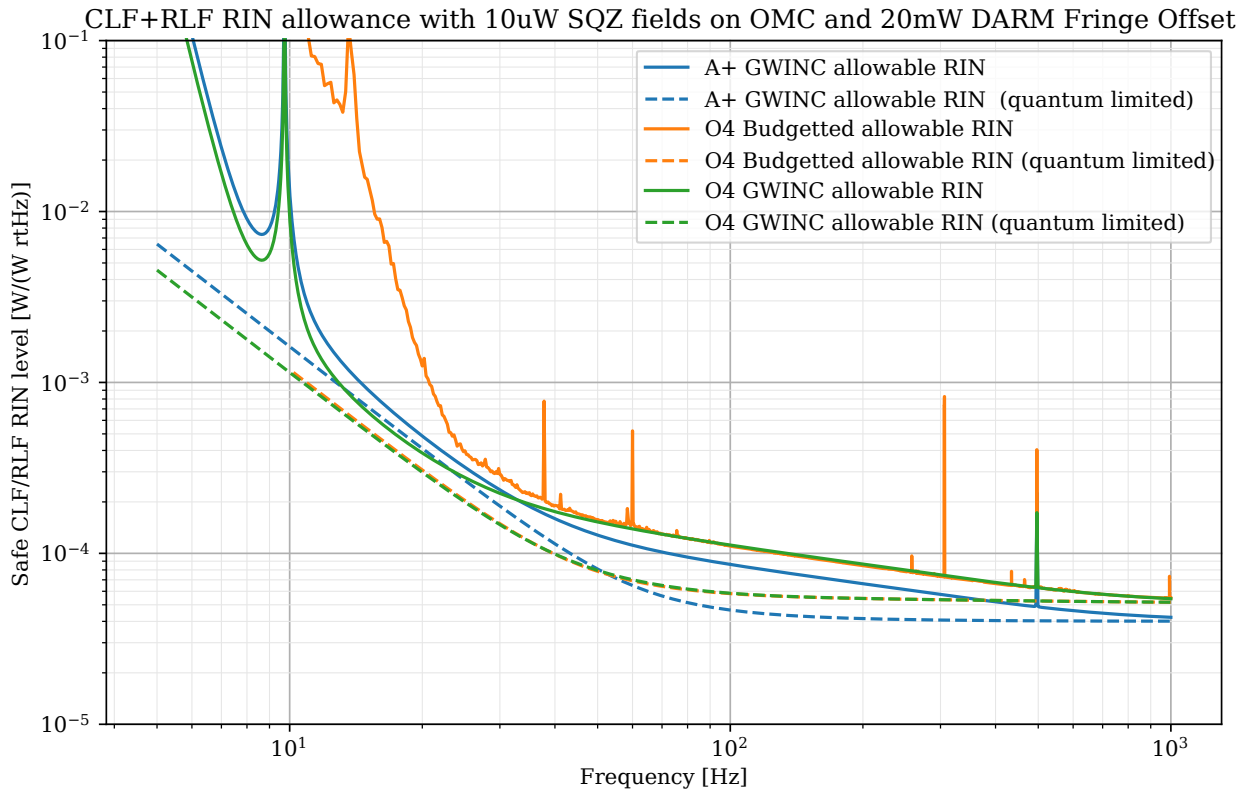


Figure 13: CLF relative intensity noise (RIN) requirements. This requirement is linear in the power level of the CLF light on the OMC.

9 Mode matching requirements

The practical improvements of squeezing are driven by the total loss of the squeezing field between generation and readout, as well as the phasing or phase noise of the squeezed field. Mode matching contributes to both losses and phasing of the squeezed beam. The phasing effects from mode mismatch are more pronounced when matching frequency dependent squeezing to the radiation pressure noise, as they can make sequential mode mis-matches degrade the shot noise more than the sum of each mismatch loss. This is shown in figures below through the spread of the mode-mismatch contribution to the quantum noise budgets.

The series of potential mode matching requirements relevant to the squeezer are:

- the squeezed beam produced by the **OPO** needs to be well mode-matched to the **FC**;
- the squeezed beam reflected off the **FC** needs to be well mode-matched to the **IFO**.
- The **IFO** should be well-match to the **OMC**.

We therefore require two different mode-matching telescopes for the squeezed beam:

- a mode-matching telescope between the **OPO** and the **FC**;
- a mode-matching telescope between the **FC** and the **IFO**

In addition to the existing third mode matching telescope, between the **IFO** and the **OMC**, which is common between the **IFO** beam and the squeezed beam. Operationally, we envision this third telescope to be tuned first, to maximize the mode match of the **IFO** beam to the **OMC** to at least 98% level, and the telescope between the **FC** and the **IFO** to be adjusted afterwards to correct for any remaining mismatch of the squeezed beam to the **OMC**.

We use the code developed in [1] to calculate the impact of mode mismatch to the **FC** performance, assuming the baseline parameters summarized in table 2, described in the previous sections.

FC length	300 m
FC round-trip loss	60 ppm
Amount of injected squeezing	12 dB
Frequency-independent phase noise	30 mrad
Injection loss (from OPO to IFO, excluding mode-mismatch)	5%
Readout loss (from IFO to OMC, excluding mode-mismatch)	10%

Table 2: Set of baseline parameters used to calculate the impact of mode-mismatch to the **FC** performance.

Fig. 14 shows the **FC** performance for different mode-matching levels and two different **FC** length noise levels, 2.5pm and 0.7pm (as described in Sec. 11). In particular:

- Figs. 14a 14b show how an optimal mode matching between the **OPO**, the **FC** and the **OMC** would allow exceeding the 6 dB broadband squeezing target;
- Figs. 14c 14d show the minimal squeezing degradation at low frequency by introducing a mode mismatch of 2% between the **OPO** and the filter cavity, and 2% mode mismatch between the **FC** and the **OMC**;

- Fig. 14e 14f show a larger degradation at low frequency by introducing a mode mismatch of 4% between the **OPO** and the **FC**, and the **FC** and the OMC.

To interpret these plots, consider the goal of 6db broadband squeezing where A+ will be shot noise limited, and consider that we will have mode matching actuators. The mode matching degradation is provided as a range as it is affected by the relative phasing in the interference of HG02 with the carrier HG01 at each mismatch site. We are assuming that with the actuation freedom designed into the telescopes, that the relative phasing of the mismatch may be tuned for the best-case at a given mismatch. While the best case at 96% matching does exceed the goal 6db at 50Hz, this is also where the **IFO** is **Coating Thermal Noise (CTN)** limited, and so the practical effect from this degradation is limited.

Based on this analysis, **we require the mode matching to be at least 96% between **OPO** and **FC**, and **FC** and **OMC**.**

9.1 Active mode matching implementation

AWC is required for all of the above telescopes in order to ensure in-situ optimal tuning.

As described in 6.5, the back scattered light noise requirement imposes that the relay optics of the mode-matching telescopes in the squeezed beam path are suspended by at least one single stage suspension.

An additional document will detail the optical layout in full detail. Some additional considerations known at the time of this writing:

- The SQZ to **FC** to IFO paths are all thermally stable, and should not change with time. The **FC** to IFO path may change to compensate for the IFO or to compensate for IFO mode actuators such as the SRM heater.
- As such, the principle mode matching of the squeezer is to perfect static matching, rather than follow thermal state.
- The SQZ to **FC** path requires at least 3 actuators due to spacing constraints on the ISI, and the beamsize coupled to the cavity. Of these, the two nearest the cavity must have degenerate Gouy phase to expand the beam rapidly, and so only the stage nearest to the cavity should be instrumented with AWC as it has the largest beamsize.
- The SQZ to **FC** Actuator nearest the squeezer will have a sufficiently small beamsize that a lens translation stage on the **OPOS** may provide the strongest mode actuation.

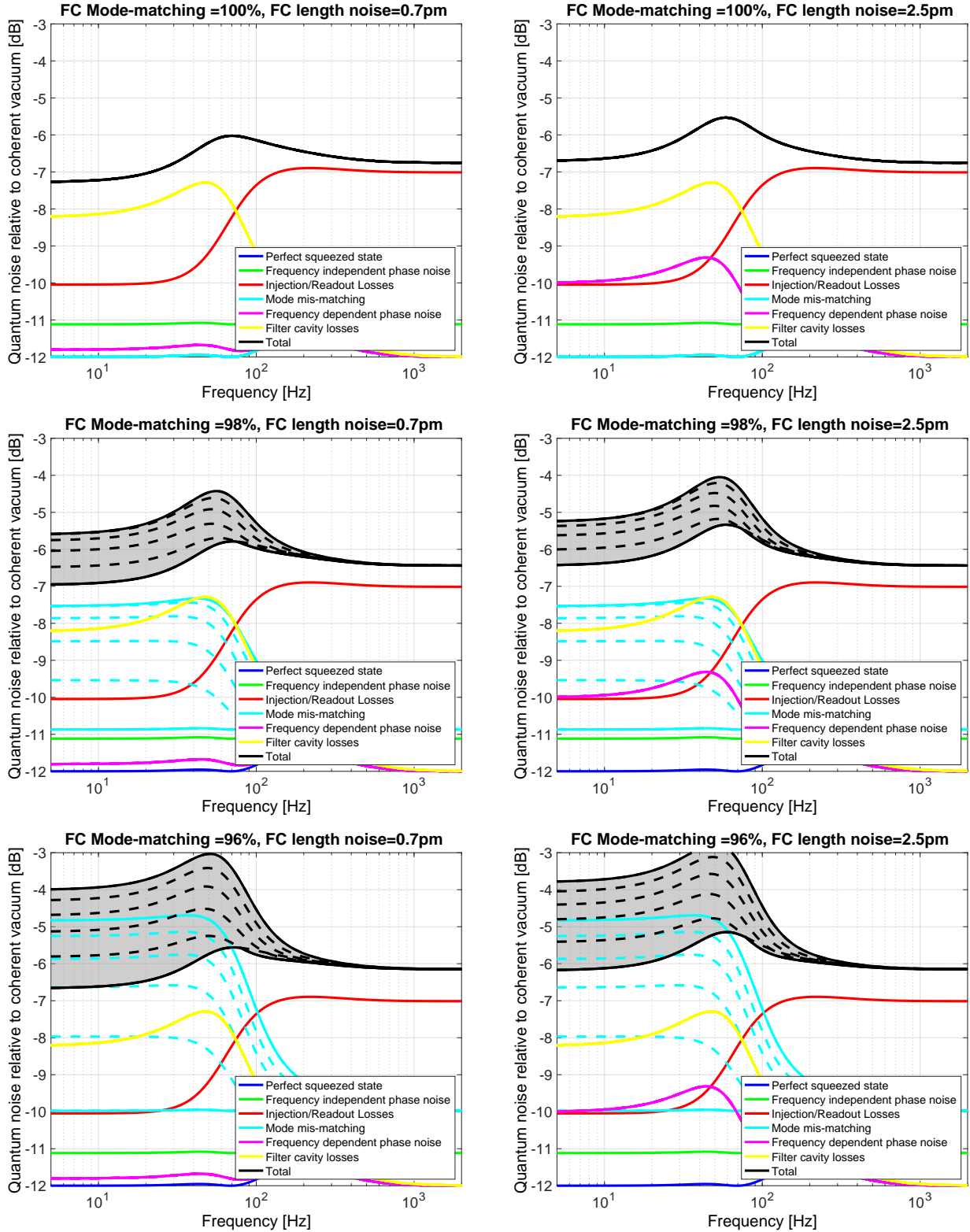


Figure 14: Impact of mode mismatch on the FC performance. For simplicity, we present plots with the same level of mode-mismatch (optimal, 98% and 96% mode matching) for the two mode-matching telescopes (OPO-FC and FC-OMC), with the matching between the IFO and the OMC optimal in all cases.

10 Beam size requirements

Two constraints drive the beam size requirements on the **FC** optics and on the relay optics. The main one is clipping loss, particularly inside the **FC**. The large beam required for a 300m cavity places some restrictions on the mode matching solutions possible.

The clipping loss may be calculated by integrating the total beam power outside of the aperture. Using the aperture diameter and the standard beam 2σ intensity diameter (twice the beam “width” w), gives:

$$\Lambda_{\text{clip}} = C_{\text{diffract}} \frac{1}{2} e^{-2d_{\text{optic}}^2/d_{\text{beam}}^2} \quad (19)$$

This may be modified to calculate clipping from a mis-centering by distance l_{center} using an effectively smaller aperture, along with dividing by two to account for no clipping on the side opposite the mis-centering

$$\Lambda_{\text{clip}} = C_{\text{diffract}} \frac{1}{2} e^{-2(d_{\text{optic}} - 2 \cdot l_{\text{center}})^2/d_{\text{beam}}^2} \quad (20)$$

The second requirement is backscatter noise from beam jitter interacting with clipping loss.

The constant C_{diffract} is included to add additional diffraction clipping loss past the simple mode clipping model. This loss is known from FFT simulations of the arm cavities (see slide 11 of [G080084](#)). From studies of the arm cavities this factor is $C_{\text{diffract}} \approx 2.5$. This value should be pessimistic, given that the arm cavities use beams widths that are a larger fraction of the optic size than intended for the filter cavity optical design.

10.1 Filter Cavity optics

The clipping losses in the cavity must be low compared to the already minimal 60ppm of scattering/coating losses of the mirrors. Following the wisdom that the beam diameter should stay 5x smaller than the 6in optic diameter gives a 30mm beam diameter. This is easily met even with a flat-curved geometry cavity.

For a 30mm beam on a 6" (153mm) optic, the scattering loss is minuscule. A better rubric is how mis-centered may the beam before accumulating 1ppm of loss. For these parameters, the beam center can be as much as 1.5" (38mm) from the center and still maintain lower than 1ppm of clipping loss.

$$\Lambda_{\text{clip}} = \frac{1}{2} e^{-2(153\text{mm} - 2 \cdot 38\text{mm})^2/(30\text{mm})^2} = 1 \cdot 10^{-6} \quad (21)$$

10.2 Relay Optics

The relay optics will generally be 2" optics with 1-2mm beams on them, in which case clipping is exceptionally small. This section discusses the requirement on relay optic nearest the **FC**, which current layouts place 44" from the 20mm diameter cavity beam. For this optic:

- the beam must be focused to a reasonable size from the large **FC** beam, requiring the cavity optic to have a curved AR surface to lens the beam. The 6" cavity optic should not have too excessive a saggita for this lens, so a requirement is necessary.

- To scan the **FC** axis transverse position, the beam will also scan on this relay optic.

The desire to scan 1" on the FC1 optic is excessive for the smaller relay optic, so the expectation is that a lowest-loss position will be established in the cavity, and then the relay optic will be repositioned to center the relay on the appropriate beam axis. After this repositioning, we expect the beam to be within 0.5" of the center. While this is easy on the horizontal axis, if the cavity axis require substantial vertical translation, this relay optic may require alternate elevation. This should be possible as the relay optics suspensions will be raised to match beam heights with the **HSTS** of the cavity. With this limit on the mis-centering, the double-pass loss through the optic with a 15mm beam is:

$$\Lambda_{\text{clip}} = e^{-2(50.8\text{mm} - 2 \cdot 12.7\text{mm})^2/(15\text{mm})^2} = 3.2 \cdot 10^{-3} \quad (22)$$

and with this clipping loss also comes a requirement on the beam jitter, assuming 4m between the **OPOS** focusing elements and this relay optic transporting the large beam:

$$S_{\text{jitter}} = \frac{d\Lambda_{\text{clip}}}{d l_{\text{center}}} = 1.5\text{m}^{-1} \quad (23)$$

$$N_{\text{jitter}}(f) \leq C_{\text{safe}} C_{\text{sqz}} \frac{Q_\lambda}{S_{\text{jitter}} \cdot 4\text{m} \cdot \sqrt{P_{\text{leak}}}} \quad (24)$$

$$\leq 0.7 \frac{\mu\text{Rad}}{\sqrt{\text{Hz}}} \left(\frac{P_{\text{leak}}}{50\text{pW}} \right)^{-1/2} \quad (25)$$

Which is substantially larger than the sensitivity of OSEMs to angles on an **HTTS** or of the angular noise of the ISI, so jitter on backscatter should not drive the requirement given this beam size.

10.3 Beam Tubes

The apertures through the beam tubes should also be considered for clipping loss of the cavity beam, with an additional safety factor to allow freedom in scanning the optic for a lowest loss cavity axis. For this freedom, we would like to maintain the ability to scan $\pm 1\text{in}$ (25mm) from the nominal beam position. This limits any aperture to a clear area 2.5" (63mm) from the nominal axis at the center of the **FC** optics. Accounting also for the double-passing, the clipping calculation is:

$$\Lambda_{\text{clip}} = e^{-2(2 \cdot 63\text{mm} - 2 \cdot 25\text{mm})^2/(30\text{mm})^2} = 2.5 \cdot 10^{-6} \quad (26)$$

3" (76mm) is a more comfortable limit, providing the same aperture as the optics.

This requirement is additionally driven by beam jitter requirements and alignment control capabilities of the cavity. The amplitude modulation from jitter-driven clipping loss is cavity-enhanced, and enhanced by length of the cavity length. For a flat-curved geometry with a ROC of 500m on FC2, angular motion the flat optic is scaled by 300m and the curved optic by the ROC. The cavity enhancement applies to both the backscatter field and the sideband field,

$$S_{\text{jitter}} = \frac{d\Lambda_{\text{clip}}}{d l_{\text{center}}} = 8.4 \cdot 10^{-4} \text{ m}^{-1} \quad (27)$$

$$S_{\text{cavity}} = \frac{t_1^2}{(1 - r_{\text{rt}})^2} = \frac{c}{2\pi L_{\text{FC}} f_p} \quad (28)$$

$$N_{\text{jitter}}(f) \leq C_{\text{safe}} C_{\text{sqz}} \frac{Q_\lambda}{S_{\text{cavity}} S_{\text{jitter}} \cdot 500 \text{m} \cdot \sqrt{P_{\text{leak}}}} \quad (29)$$

$$\leq 3 \frac{\text{nRad}}{\sqrt{\text{Hz}}} \left(\frac{P_{\text{leak}}}{50 \text{pW}} \right)^{-1/2} \quad (30)$$

Which, while quite small, is lower than the current angular noise in the IMC. If the length scale is removed in the above equation, the length noise of the apertures for beam clipping is computed

$$N_{\text{aperture}}(f) \leq C_{\text{safe}} C_{\text{sqz}} \frac{Q_\lambda}{S_{\text{cavity}} S_{\text{jitter}} \cdot \sqrt{P_{\text{leak}}}} \quad (31)$$

$$\leq 1.6 \frac{\mu\text{m}}{\sqrt{\text{Hz}}} \left(\frac{P_{\text{leak}}}{50 \text{pW}} \right)^{-1/2} \quad (32)$$

10.4 Baffling

The FC will require some level of baffling to the possibility that ground motion in the vacuum enclosures couples optically to either the backscatter and sensing fields. The requirements are set from the backscatter performance, as well as the total length RMS of the cavity. The cavity enhances optical couplings through the round-trip gain of the cavity, which can modulate the backscatter field to cause noise, or it can modulate the sensing field to generate sensing noise, which is then injected through the control loops.

To calculate this we need to estimate the BRDF of the mirrors, the BRDF of the surrounding baffle or beamtube material, and kinematic factors for the scattering off of mirrors to baffles, off of baffles to mirrors, and finally from mirrors into the beam. All of these factors can be wrapped into a triple integral and reduced down to the condensed form used in eq. 17 of T940063 as

$$S_{\text{diffuse}}^2 = \int_0^{2\pi} \int_0^{\frac{\pi}{2}} \frac{\lambda^2}{r^2(\theta)} B_o^2(\theta) B_t(\theta + X) \sin(\theta) d\theta d\phi \quad (33)$$

where S_{diffuse}^2 is the power coupling of the beam in the cavity, off of surroundings and back into the beam. The factor B_o is the BRDF of the optic, and B_t is the BRDF of the tube or baffle. The additional angle X is the angle between the tube/baffle and the beamline. $r(\theta)$ is the distance of the scattering surface (tube/baffle) from the optic.

Requirements on the diffuse scattering are set from the noise they introduce on the backscatter, as well as length RMS introduced into the length sensing. Since the sensing co-propagates

with the squeezing field in the cavity, it is likely that introduced phase noise is common between them and should not affect the phase noise requirements where the loop is active, but it is worth checking how much noise is introduced nevertheless.

For the length sensing, the scale is (from eq. 18 of [T940063](#) converted from strain to length)

$$\delta l_{\text{scatter}} = S_{\text{diffuse}} \delta l_{\text{ground}} \quad (34)$$

which for the backscatter must be below the limits set in sec [6.3](#). For length noise RMS, the integrated rms of this noise within the control bandwidth must fall below the limits set in [8.1](#).

$$S_{\text{diffuse}} \leq 2.1 \cdot 10^{-16} \frac{\text{m}}{\sqrt{\text{Hz}}} \frac{1}{\delta l_{\text{ground}}(f)} \left(\frac{P_{\text{leak}}}{50 \text{pW}} \right)^{-1/2} \left(\frac{f_{\text{FC}}}{50 \text{Hz}} \right) \quad \text{for } f > 10 \text{Hz} \quad (35)$$

and then for the total RMS within the control bandwidth, the requirements are

$$S_{\text{diffuse}} \leq \frac{7.9 \cdot 10^{-13} \text{m}}{\sqrt{20 \text{Hz}}} \frac{1}{\delta l_{\text{ground}}(f)} \leq 1.8 \cdot 10^{-13} \frac{\text{m}}{\sqrt{\text{Hz}}} \frac{1}{\delta l_{\text{ground}}(f)} \quad \text{for } f < 20 \text{Hz} \quad (36)$$

Using ground motion with $1 \cdot 10^{-7} \frac{\text{m}}{\sqrt{\text{Hz}}}$ (see [T2000280](#)), gives moderately strict scatter requirements, which are more stringent from the baffle scatter noise of backscatter than the control RMS for the squeezing angle.

$$S_{\text{diffuse}} \leq 2.1 \cdot 10^{-9} \left(\frac{P_{\text{leak}}}{50 \text{pW}} \right)^{-1/2} \left(\frac{f_{\text{FC}}}{50 \text{Hz}} \right) \text{ from backscatter} \quad (37)$$

$$S_{\text{diffuse}} \leq 1.8 \cdot 10^{-7} \text{ from phase noise} \quad (38)$$

10.4.1 Scatter light level estimates

The BRDF of the mirrors may be estimated using the total scattering loss expected of the mirrors, assuming all/most of the power is distributed into some small angular scale θ_{minscale} and the remainder is uniform (Lambertian) into wide scales. The wide angle assumptions are approximately true from existing **FC** scatter measurements [\[?\]](#) and the numbers used here are pessimistic in any case. The narrow angle assumption is used since existing BRDF measurements cannot capture small angle scattering, which is known to give substantial contribution in super polished optics. The underlying phase noise of the polish has some length scale for its largest fluctuations. It may be that with polishing as good as the LIGO test-masses, that the narrow angle length scale is below the divergence angle of the FC beam. The aim of this analysis is to show that reasonable baffling strategies do not depend on that small angle scattering since we can put limits on the total mirror loss.

$$B_o(\theta) = \begin{cases} \alpha & \theta < \theta_{\text{minscale}} \\ \beta \cos(\theta) & \theta > \theta_{\text{minscale}} \end{cases} \quad (39)$$

Where we are assuming that the mirrors have low scattering loss, so

$$2\pi \int_0^{\frac{\pi}{2}} B_o(\theta) \sin(\theta) d\theta < \Lambda_{\text{rt}}/2 < 50 \cdot 10^{-6} \quad (40)$$

which sets upper limits for the scaling factors

$$\alpha < \frac{50 \cdot 10^{-6}}{\pi \theta_{\text{minscale}}^2} \quad \beta < \frac{50 \cdot 10^{-6}}{\pi} \quad (41)$$

Now to evaluate the scattering noise limits we can consider total scattering amplitudes for a near baffle wall, a tube, and a rear wall. These three cases simply change the formulation of $r(\theta)$ and the minimum and maximum radial angles used in eq. 33.

Near wall

$$r(\theta) = \frac{d_{\text{wall}}}{\cos \theta} \quad \theta_{\text{minscale}} < \theta < \pi/2 \quad (42)$$

$$S_{\text{diffuse}} < \sqrt{\frac{\pi B_t}{4}} \beta \frac{\lambda}{d_{\text{wall}}} < 4 \cdot 10^{-5} \sqrt{B_t} \frac{\lambda}{d_{\text{wall}}} \quad (43)$$

which meets the requirements for a near wall of sufficient distance.

Beam tube

$$r(\theta) = \frac{d_{\text{tube}}}{2 \sin \theta} \quad 0 < \theta < \pi/2 \quad (44)$$

$$S_{\text{diffuse}} < \sqrt{\frac{\pi B_t}{4}} \frac{\lambda}{d_{\text{tube}}} \sqrt{\beta^2 + \alpha^2 \theta_{\text{minscale}}^4} < 6 \cdot 10^{-5} \sqrt{B_t} \frac{\lambda}{d_{\text{tube}}} \quad (45)$$

which meets the requirements for a beam tube of with a 6 in diameter, though only within a factor of 10 assuming a large BRDF.

Far wall

$$r(\theta) = \frac{L_{\text{FC}}}{\cos \theta} \quad 0 < \theta < \theta_{\text{minscale}} \quad (46)$$

$$S_{\text{diffuse}} < \sqrt{\frac{\pi B_t}{4}} \alpha \theta_{\text{minscale}}^2 \frac{\lambda}{L_{\text{FC}}} < 2 \cdot 10^{-13} \sqrt{B_t} \quad (47)$$

which is extremely small.

Altogether, these calculations suggest that only wide angle scattering contributes to length noise, and so a simple near wall baffle should be installed.

10.5 Specular scatterering

Given the apparent lax requirements for baffling, the only remaining concern may be specular scattering, which can couple large amounts of light between the mirrors through external surfaces. Specular scatter from some distance must refocus the beam back to the original

point, this implies (by unit analysis) a surface with a BRDF that is enhanced to cancel the mirror cross section factor $\frac{\lambda}{r(\theta)}$.

$$S_{\text{specular}}^2 = \int_0^{2\pi} \int_0^{\frac{\pi}{2}} B_o^2(\theta) B_s(\theta + X) \sin(\theta) d\theta d\phi \quad (48)$$

Where $B_s(\theta)$ is the reflectance function for specular scatterers. It is order 1 where such scattering exists and 0 elsewhere. It primarily measures the area of specular scatterers. Assuming that the only specular scattering at narrow angles is the optic, then the total coupling for specular scatter is:

$$S_{\text{specular}}^2 < A_{\text{specular}} (50 \cdot 10^{-6})^2 \quad (49)$$

and so the total area of specular scattering from vacuum seams or baffle edges must be smaller than $\frac{1}{50}$ of a steradian to meet the requirements. This should be easily met.

10.5.1 Baffle Implementation

Given the rather minimal requirements for scatter from the beam tube, we propose that a limited number of baffles to be installed only to prevent specular reflection down the tubes. For baffles occupying 1/4 of the tube radius, say 1in baffles in a 8in diameter tube, only 5 baffles should be needed to prevent the beam from seeing the far mirror via reflections from the tube. This configuration will allow the beam to see the first half of the tube, which may have seems from vacuum connections. As long as these take up sufficiently small area specular reflections from seams will not impact the [FC](#) operation.

Since the scattering on near surfaces comes the closest to violating the requirement, we recommend a simple mirror baffle mounted on the ISI in front of each cavity optic with an aperture equal to the mirror diameter.

10.6 Diffractive Baffle Scattering

This section is a copy of [T2000476](#) to keep everything in one place.

The following equations are based off of [T950101](#) eq. 4, which gives the scatter coupling into strain including phase factors for the light. Just following that equation is a section that outlines all of the parameters, and the equation can be converted to the following form. In practice, the most convenient parameters available to characterize the scattering from an optic is its [Bi-directional reflectance distribution \(BRDF\)](#). For this document, only one-direction is necessary as the optic is illuminated by a coherent laser beam, so the [BRDF](#), $B_O(\theta, \phi)$ indicates the fractional power scattered into unit solid angle at radial angle θ and azimuthal angle ϕ . The azimuthal angle is often dropped as it averages to a constant assuming azimuthally symmetric randomness of mirror surfaces.

The important point of [T950101](#) is that the phasing of the scattered light can be expected to be slowly varying across the baffle edge, due to diffraction smoothing out the phase front from the optic. Due to this, motion of the baffle can strongly modulate the coupling from one mirror to another from the variations in the overlap integral of the scattered light. Serrations

may be added to generate phase modulations that average away the overlap integral of a modulating aperture.

This document primarily derives the noise component without serrations, using the [BRDF](#). This allows a quick calculation of the magnitude of the problem if serrations are omitted. The [BRDF](#) is additionally useful because it is related to the total scatter loss of the optic, and expectations of that loss constrain scattering models.

The length noise from a single baffle between two optics is:

$$\delta l_{FC} \leq \frac{\lambda R \sqrt{B_o(\theta_n)B_o(\theta'_n)}}{\pi l_n(L - l_n)} \delta X_{\text{baffle}} \quad (50)$$

where l_n is the distance down the tube of the baffle. R is the radius of baffle aperture. $L = 300\text{m}$ is (approximately) the tube length and $B_o(\theta_n)$ is the [BRDF](#) of the optic surface for the opening angle of the n^{th} baffle. The angles θ_n and θ'_n are the polar angles of the baffle apertures from each respective optic and baffle faces.

$$\theta_n = \frac{R}{l_n} \quad \theta'_n = \frac{R}{300\text{m} - l_n} \quad (51)$$

Dennis's document [T2000280](#) outlines that the horizontal motion of the tubes/baffles can be expected to be in the few $10^{-8} \frac{\text{m}}{\sqrt{\text{Hz}}}$, so we will assume $\delta X_{\text{baffle}} \leq 10^{-7} \frac{\text{m}}{\sqrt{\text{Hz}}}$. Given expected backscatter, the filter cavity has the length noise requirement $\delta l_{FC} \leq 2 \cdot 10^{-16} \frac{\text{m}}{\sqrt{\text{Hz}}}$ at which optical modulations are sufficiently hidden from the interferometer. This factor includes a safety factor of 10 and the squeezing level. This gives the requirement:

$$\frac{\delta l_{FC}}{\delta X_{\text{baffle}}} \leq S_{\text{diffraction}} \leq 2 \cdot 10^{-9} \quad (52)$$

The formula for $S_{\text{diffraction}}$ ultimately depends on all of the baffles down the tube, and can be considered as a worst case, where all of the baffles coherently add

$$S_{\text{diffraction}} = \sum_{n=0}^N \frac{\lambda R \sqrt{B_o(\theta_n)B_o(\theta'_n)}}{\pi l_n(300\text{m} - l_n)} \quad \text{or} \quad S_{\text{diffraction}} = \sqrt{\sum_{n=0}^N \left| \frac{\lambda R \sqrt{B_o(\theta_n)B_o(\theta'_n)}}{\pi l_n(300\text{m} - l_n)} \right|^2} \quad (53)$$

10.6.1 Plots assuming different BRDFs of the mirrors

In this section, various BRDF models are plugged into the formulas above to determine the apparent length noise arising from baffle modulations. All models use a θ^{-2} dependence at low frequencies, as this dependence can be considered maximally bad. Any faster θ^{-3} or more and the rolloff is so fast that the θ ' contribution is minimal (or the total scatter becomes unrealistic). Any slower like θ^{-1} and the θ contribution is very small for realistic total scatter. In any case, random mirror maps of the optic surface seem to indicate that θ^{-2} is a reasonable angle dependence.

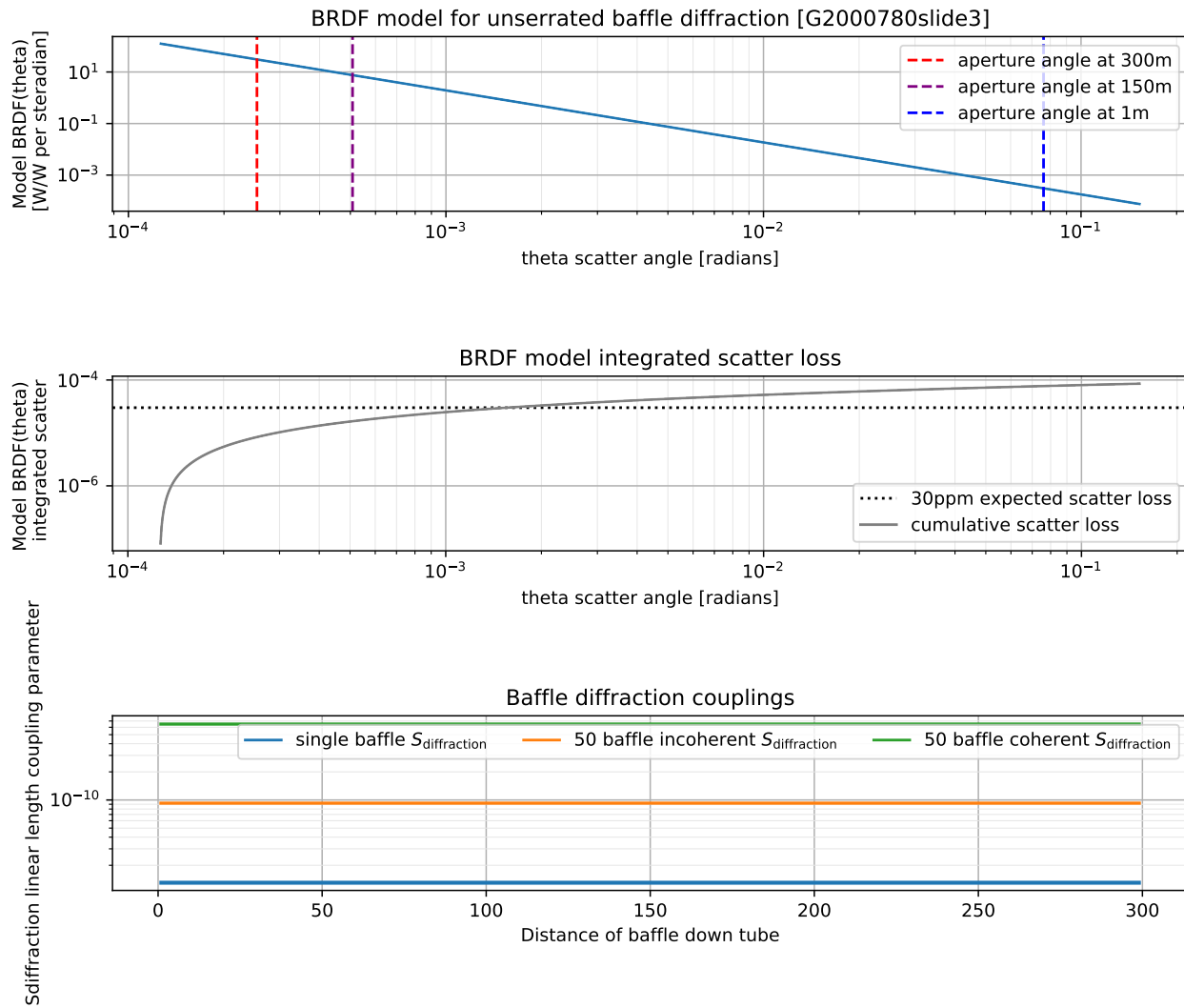


Figure 15: This model uses $B_O(3\text{in}/300\text{m}) \approx 80$ as shown in slide 3 of [G2000780](#), which also appears to model a similar θ^{-2} dependence to the scatter power.

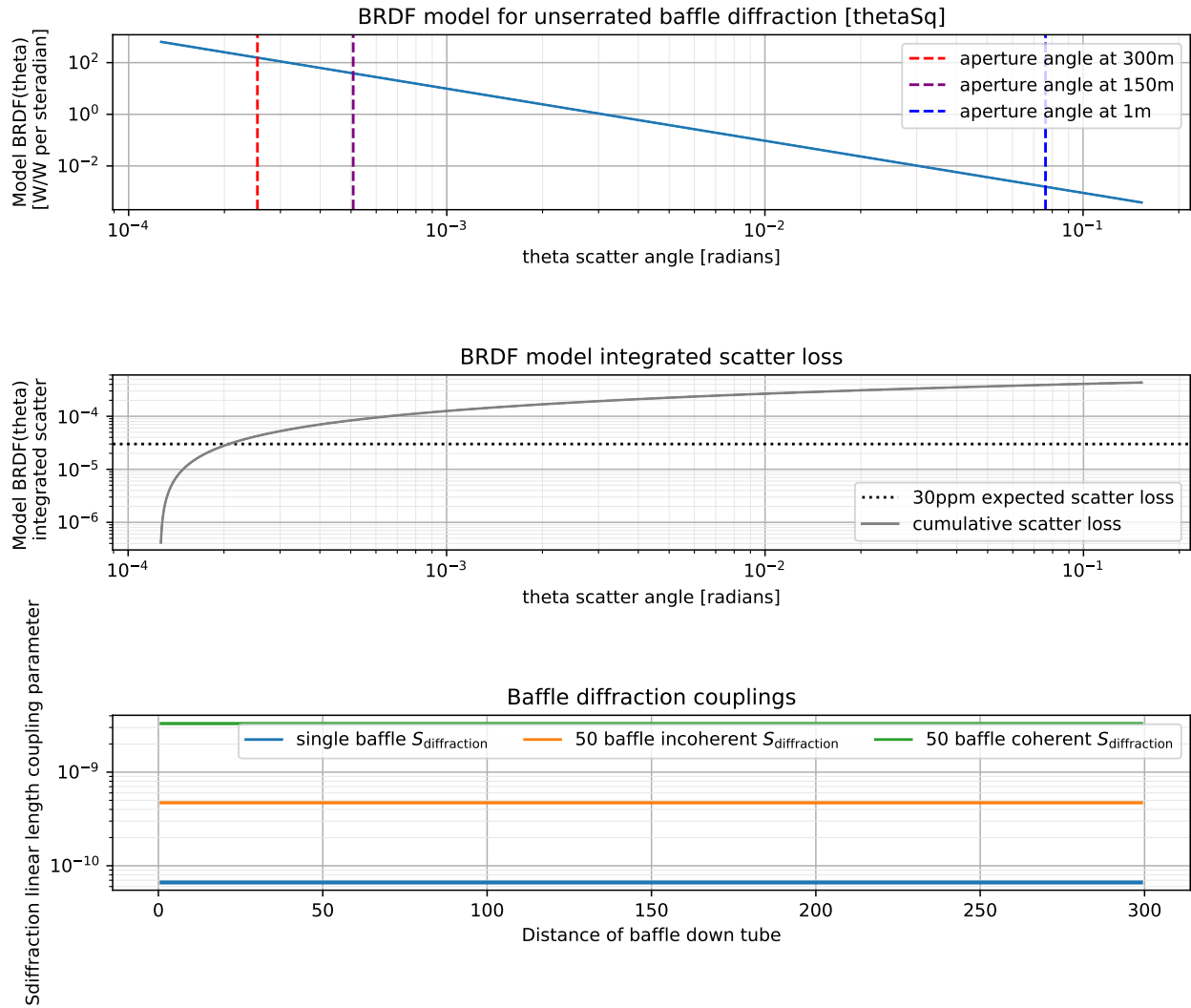


Figure 16: This BRDF uses a worst case BRDF of $30\text{ppm}/\pi\theta^2$, which causes any/all θ to saturate the expected loss.

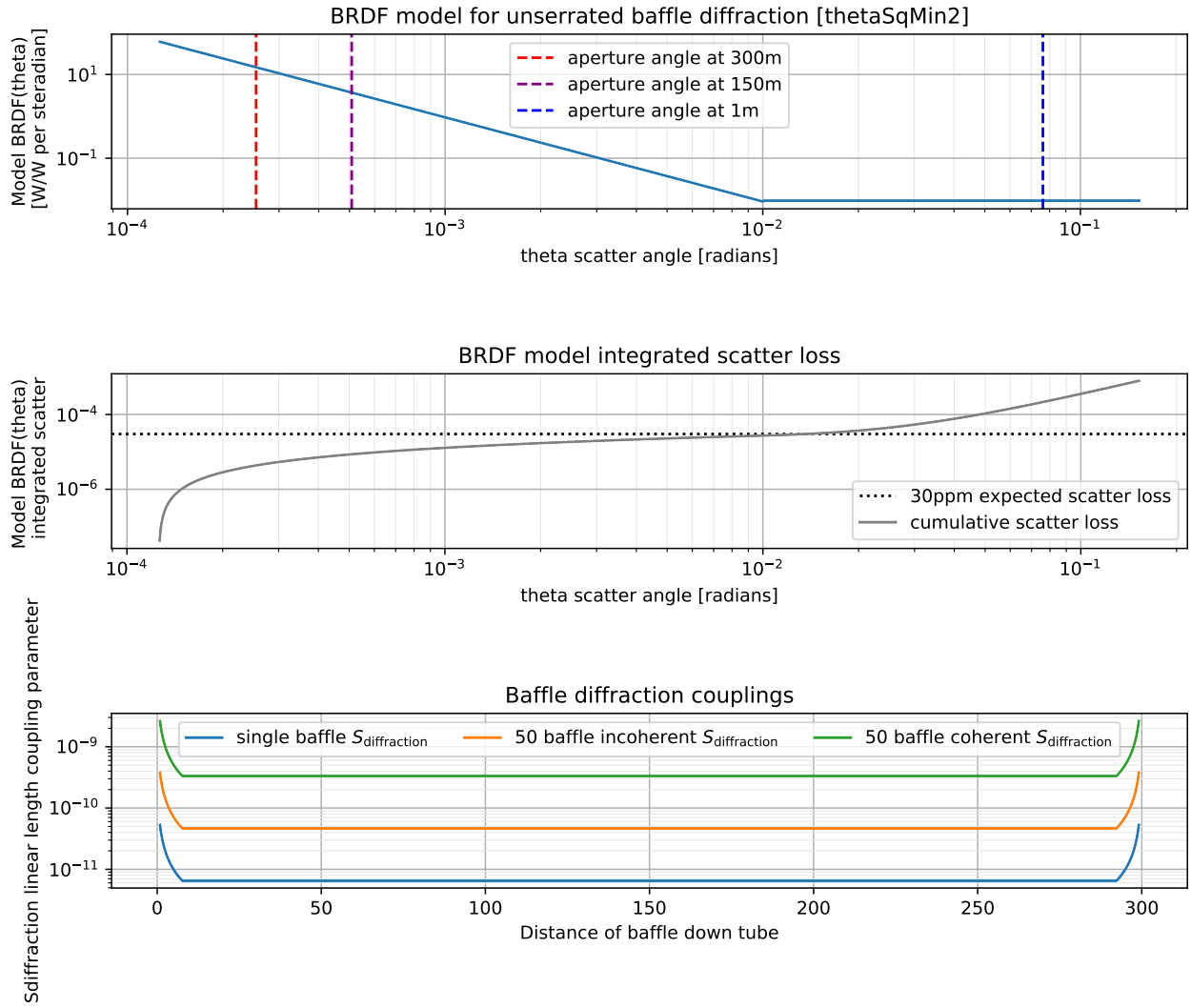


Figure 17: This BRDF uses a BRDF of $30\text{ppm}/10\pi\theta^2$, scaled to not violate the loss expectation. Then it cuts off the roll off for a constant reflectance. This causes it to violate the loss expectation, but in a manner that investigates the influence of intermediate angle scattering.

10.6.2 Derivation

This section derives the equations used above by relating the field distribution along any z -plane down the tube from the input optic FC1 $U_{FC1}(x, y, z)$ back to the BRDF of the optic.

The field overlap of the field plane is calculated using an overlap integral with a masking function $m(x, y)$ that depends on the modulating lateral displacement δX of the baffle.

$$A = \int_{-\infty}^{\infty} \int_{-\infty}^{\infty} m(x, y) dx dy = 4R\delta X \quad (54)$$

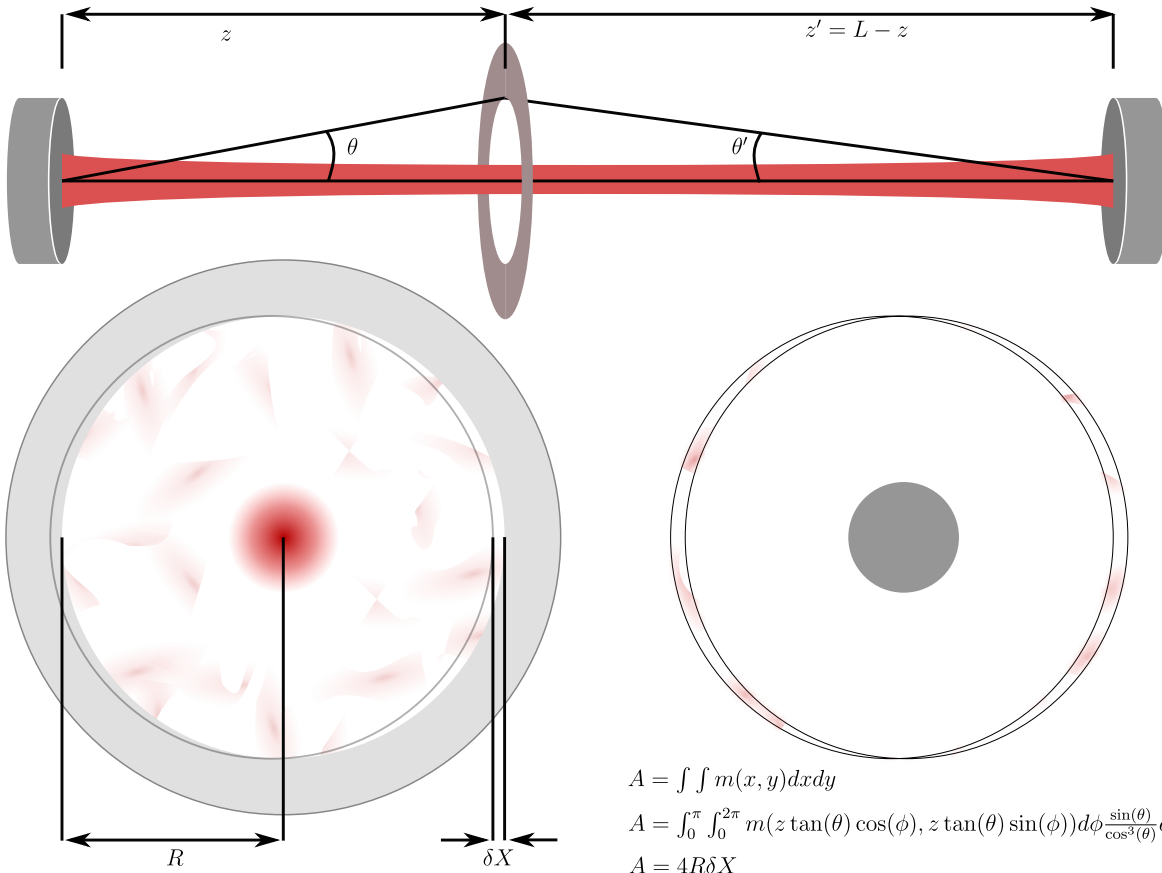


Figure 18:

Down the tube there is the beam field profile for each mirror $U_{FC1}(x, y, z)$ and $U_{FC2}(x, y, z')$. These fields can be related to a nominal fundamental mode U_{00} and the scatter is related to deviation of the field from the fundamental, which is expressed as U_{diff1} and U_{diff2} .

$$U_{FC1}(x, y, z) \approx U_{00}(x, y, z) \quad (55)$$

$$1 = \int_{-\infty}^{\infty} \int_{-\infty}^{\infty} |U_{FC}(x, y, z)|^2 dx dy \quad (56)$$

$$1 = \int_{-\infty}^{\infty} \int_{-\infty}^{\infty} |U_{00}(x, y, z)|^2 dx dy \quad (57)$$

$$U_{diff1}(x, y, z) = U_{FC1}(x, y, z) - U_{00}(x, y, z) \quad (58)$$

To relate this field deviation profile to the BRDF, we must change coordinates and account for the volume elements since the field profile and BRDF are both densities. The coordinate transformation is:

$$x = z \tan(\theta) \cos(\phi) \quad y = z \tan(\theta) \sin(\phi) \quad (59)$$

And the two are then related by:

$$B_o(\theta, \phi) \sin(\theta) d\phi d\theta = |U_{FC1}(x, y, z) - U_{00}(x, y, z)|^2 dx dy \quad (60)$$

$$B_o(\theta, \phi) \sin(\theta) = |U_{\text{diff1}}(z \tan(\theta) \cos(\phi), z \tan(\theta) \sin(\phi), z)|^2 z^2 \frac{\sin(\theta)}{\cos^3(\theta)} \quad (61)$$

$$B_o(\theta, \phi) \approx |U_{\text{diff1}}(z \tan(\theta) \cos(\phi), z \tan(\theta) \sin(\phi), z)|^2 z^2 \quad (62)$$

With the BRDF and field profile established, we can write the exact modulation coupling, c , of the fields from the two optics from the masked overlap integral. This coupling can then be related to an equivalent effective length modulation.

$$c = \int_{-\infty}^{\infty} \int_{-\infty}^{\infty} m(x, y) U_{\text{diff1}}(x, y) U_{\text{diff2}}^*(x, y) dx dy \quad (63)$$

$$\delta L = \frac{\lambda}{4\pi} |c| \quad (64)$$

Of course, we do not know U exactly, so we can set an estimate, C , using the expected magnitude of U . This removes the phase modulation that causes cancellations in the overlap integral.

$$|c| \leq C = \int_{-\infty}^{\infty} \int_{-\infty}^{\infty} m(x, y) |U_{\text{diff1}}(x, y) U_{\text{diff2}}^*(x, y)| dx dy \quad (65)$$

This can then be related back the [BRDF](#) and simplified.

$$C = \int_{-\infty}^{\infty} \int_{-\infty}^{\infty} m(x, y) \sqrt{\frac{B_o(\theta(x, y, z), \phi(x, y))}{z^2}} \sqrt{\frac{B_o(\theta'(x, y, z), \phi(x, y))}{(L-z)^2}} dx dy \quad (66)$$

$$\approx \frac{4R\delta X}{z(L-z)} \sqrt{B_o(\theta) B_o(\theta')} \quad (67)$$

Finally, the coupling limit C is exactly $S_{\text{diffraction}}$ from the first section.

$$\delta L \leq \frac{\lambda R \sqrt{B_o(\frac{R}{z}) B_o(\frac{R}{L-z})}}{\pi z (L-z)} \delta X \quad (68)$$

11 Sensing Frequency Requirements

The filter cavity must be sensed from fields offset from the carrier, while maintaining its controls and length requirements. At least one of the sensing fields must resonate in the cavity to generate a length signal. Furthermore, a length sensing which co-propagates with the squeezing field may only be read out at high sensitivity in the interferometer [BHD](#) or

DC photo-diodes used for interferometer readout (DCPD)s. The resonant sensing field then must be within the bandwidth of the DCPD electronics and sufficiently within the OMC bandwidth, much like the existing 3.125MHz [Coherent Locking Field \(CLF\)](#) sideband used for the squeezer. The CLF at that frequency is attenuated to 1% by the [Output Mode Cleaner \(OMC\)](#) bandwidth. Lower frequencies have the potential to inject the SQZ laser amplitude and phase noise into the interferometer, so too low of frequency should be avoided to prevent classically generated antisqueezing effects on the radiation pressure noise.

The resonant length sensing field should then be (for some integer k)

$$f_{\text{sensing}} = k \frac{c}{2L_{\text{FC}}} \pm f_{\text{det}} < 4\text{MHz} \quad (69)$$

And the [Free Spectral Range \(FSR\)](#) of a 300m filter cavity is $f_{\text{FSR}} = 499654.1\text{Hz}$.

A budget of the noise for different frequencies of sensing fields, their noise contribution back to the carrier, and intrinsic sensing noise from the generation electronics, will have to be studied.

Furthermore, any selection of this sensing frequency should also be done with knowledge of the existing environmental RF noise at the sites. For example, AM radio stations exist from 535kHz - 1605kHz and could contaminate beatnote signals with environmental RF noise.

12 Squeezed beam alignment requirements

Alignment servos needs to be implemented to keep the squeezed beam well aligned to the [FC](#) and to the [IFO](#).

12.1 Actuators

We require that the two mode matching telescopes in the squeezed beam path are designed so as to provide also a set of alignment actuators with an appropriate Gouy phase separation (at least 60 degrees, the closer to 90 degrees the better). This approach is similar to what implemented in the OMC mode-matching telescope built for Advanced LIGO ([T1000317](#)).

12.2 Sensors

The alignment of the squeezed beam to the [IFO](#) beam can be sensed by the ASC_AS wave-front-sensors, as done in the Advanced LIGO set-up, where we detect on the two AS WFSs the beat between the 45.5 MHz sidebands (local oscillator) and the 3.1 MHz coherent locking field (signal), at 42.4 MHz. Assuming this strategy is successful in Advanced LIGO, the same approach will be used in A+.

A set of additional WFSs need to be installed to be able to align the squeezed beam to the [FC](#).

13 Coating Parameters

This section is to concisely summarize the parameters for the filter cavity coatings and justify their tolerances. The Arm power dependence analysis in the appendix also analyzes

the sensitivity of the filter cavity optimum to the operating power, but does not choose an optimal operating point in the 450-500kW range.

This is a more exact study than the general linewidth requirements detailed in previous sections. Note that the mirrors here are labeled FC1 and FC2 as designated in the layout drawings and assigned for the suspensions; however, the substrate, coating and polish documents use FIM (Filter Cavity Input Mirror) for FC1 and FEM (Filter Cavity End Mirror) for FC2.

- FC1 Surface 1 at 1064nm: $0.001 \pm 5\%$ Transmissivity HR
- FC2 Surface 1 at 1064nm: 2-4 ppm Transmissivity HR

The transmissivity of the input mirror FC1 is determined by running GWINC and optimizing the range as a function of the squeezing level and transmissivity. These are shown in Figures 19 and 20. The optimization is performed as a function of the input power, but the power in the arms determines the sensitivity and the optomechanical parameters that affect the filter cavity optimum. The arm power is plotted as it is the parameter most consistent between the model and experimental measurements.

For 500kW of circulating arm power, the chosen transmissivity is optimal, and the range is a relatively weak function of the input power. This agrees with the full contour plot an analysis of [P2000240](#). This transmissivity corresponds to a filter cavity pole of 39.8Hz ideally and 42Hz with 60ppm of losses. The tolerances are set to be a relative error of 5% in the transmissivity. This will change the optimal operating point, but not severely impact the range. The transmissivity of the endmirror is chosen to be subdominant to scattering, but nonzero. Experience with the R&D filter cavity indicates that the transmission signal is useful even in operation. This range of transmissivities will cause the resonant cavity transmission to be $0.7\% \approx 4 \cdot 2 \cdot 10^{-6} / 1 \cdot 10^{-3}$ to 1.5%. This transmissivity is sufficient to be useful for backup in-air LSC or ASC sensing in transmission.

- FC1 Surface 1 532nm: 0.01 Transmissivity HR with 5% relative error
- FC2 Surface 1 532nm: 0.01 Transmissivity HR with 5% relative error

This transmissivity will form a critically coupled cavity at 532. This is optimal for RF sensing in reflection and DC sensing in transmission. The cavity pole will be 800Hz, easy to acquire lock with the 532 frequency servo. Tolerances are set so that mismatch doesn't overly ruin perfect critical coupling. At 5% mismatch with one mirror high and the other low, the cavity locked reflectivity will be 0.25 % in power. It can reach shot-noise limited sensitivity if the RF sideband modulation index is above 0.05 in the worst-case. At 532 we anticipate that the cavity will be limited by acoustic phase noise on the input sensing field, not shot noise.

All of the surface 2 coatings will be AR. As with 1064, the tolerances at 532 can be relaxed compared to 1064 if needed to meet or improve the 1064 specifications.

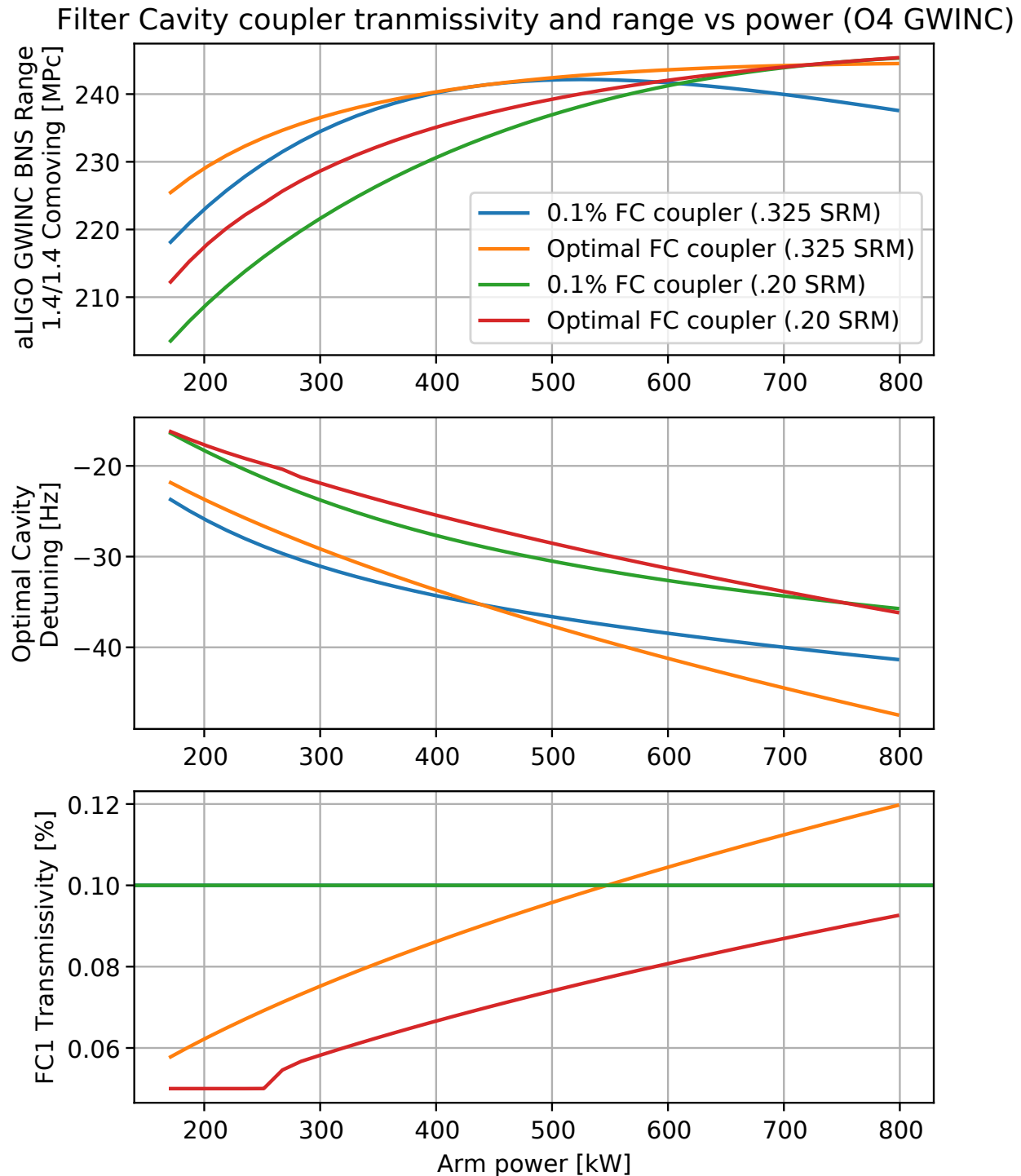


Figure 19: GWINC range calculation with the filter cavity and squeezing parameters optimized at each injected power. This uses 60ppm of round-trip loss in the cavity.

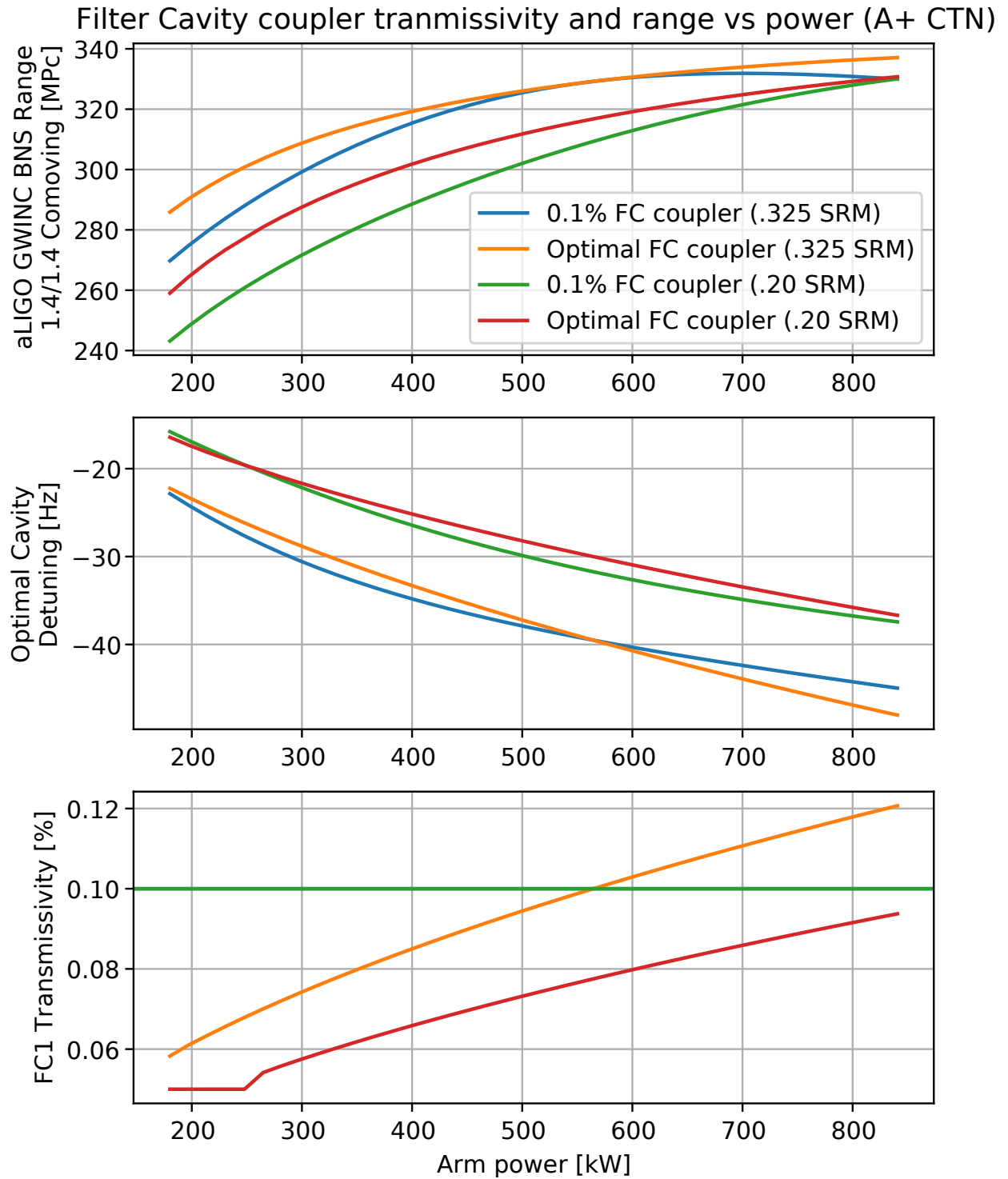


Figure 20: GWINC range calculation with the filter cavity and squeezing parameters optimized at each injected power. This plot uses the coating thermal noise assumed for A+, showing that optimum is not a function of the background noise. This uses 60ppm of round-trip loss in the cavity.

A Filter cavity performance

A.1 Filter cavity length and loss optimization

Here we study the performance of the **FC** as function of length. Fig. 21 shows the A+ inspiral range (comoving range) as function of the **FC** length in two scenarios: nominal A+ coating thermal noise (**CTN**) level and current Advanced LIGO **CTN**.

In the A+ scenario, a 100 m long **FC** corresponds to 300 Mpc. A 300m long **FC** provides about 10% more inspiral range, as well as relaxing the finesse, loss and back scatter noise requirements, as described in the first part of this document. While a 1-2 km scale **FC** would provide optimal performance of the order of 360 Mpc, this additional 10% range improvement over a 300m cavity would come at the expense of a significant larger cost of the vacuum infrastructure needed to accommodate the **FC**. The option of using the 4km **IFO** arm tubes has been considered, but discarded as it would greatly increased the complexity of the optical layout.

A 300m long **FC** seems therefore a good compromise.

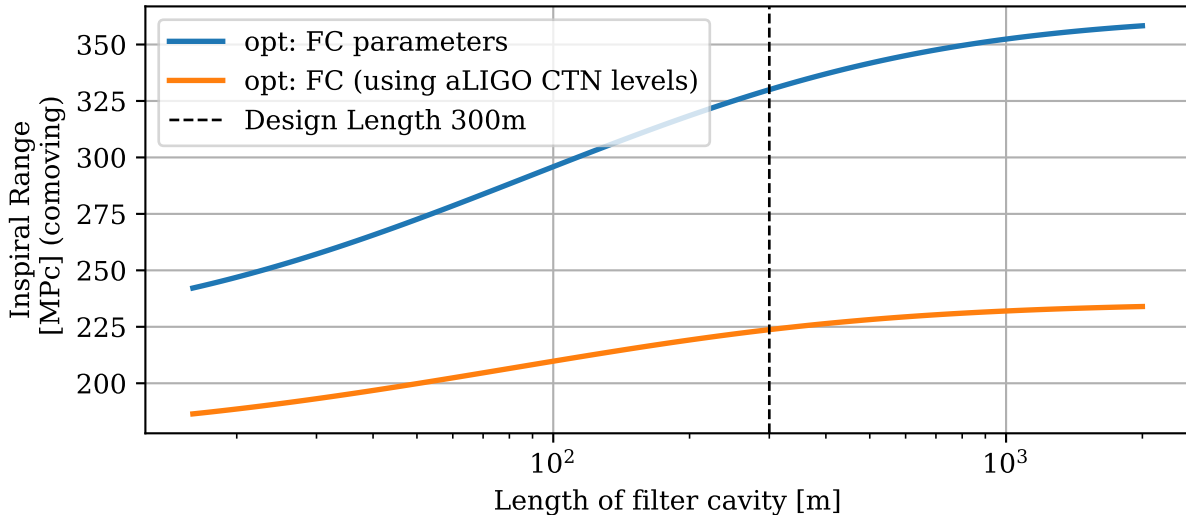


Figure 21: A+ inspiral range as function of the **FC** length. The **FC** parameters have been optimized at each length.

We also studied how the A+ inspiral range changes as function of the filter round-trip loss, for three different scenarios: **FC** input coupler with $T_{in}=1200\text{ppm}$, $T_{in}=1100\text{ppm}$ as well as an optimal transmission calculated for different round-trip loss. Although a more in depth analysis will be presented in the preliminary design document describing the **FC** parameters, we find that both T_{in} are nearly optimal for the round-trip loss of interest, with 60ppm being a realistic estimate.

A.2 Interferometer Power Dependence

Although the nominal A+ circulating power is of the order of 750 kW, the experience with Advanced LIGO is that it might be beneficial to operate intermediate configurations at lower

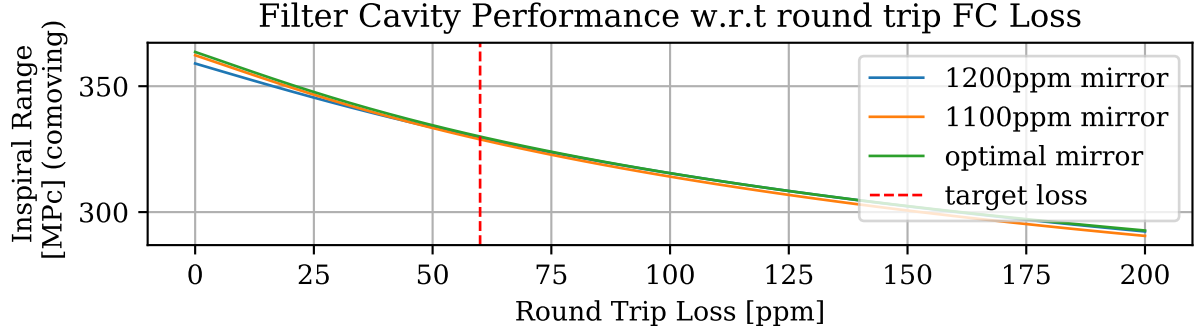


Figure 22: A+ inspiral range as function of the **FC** round-trip loss for three different scenarios: **FC** input coupler with $T_{in}=1200\text{ppm}$, $T_{in}=1100\text{ppm}$ as well as an optimal transmission calculated for different round-trip loss.

power. So here we study how critical is the choice of the **FC** input coupler transmission T_{in} if operating the **IFO** at different power levels. We use the scenarios described in the previous section: $T_{in}=1200\text{ppm}$, $T_{in}=1100\text{ppm}$ as well as an optimal transmission calculated for different circulating power levels.

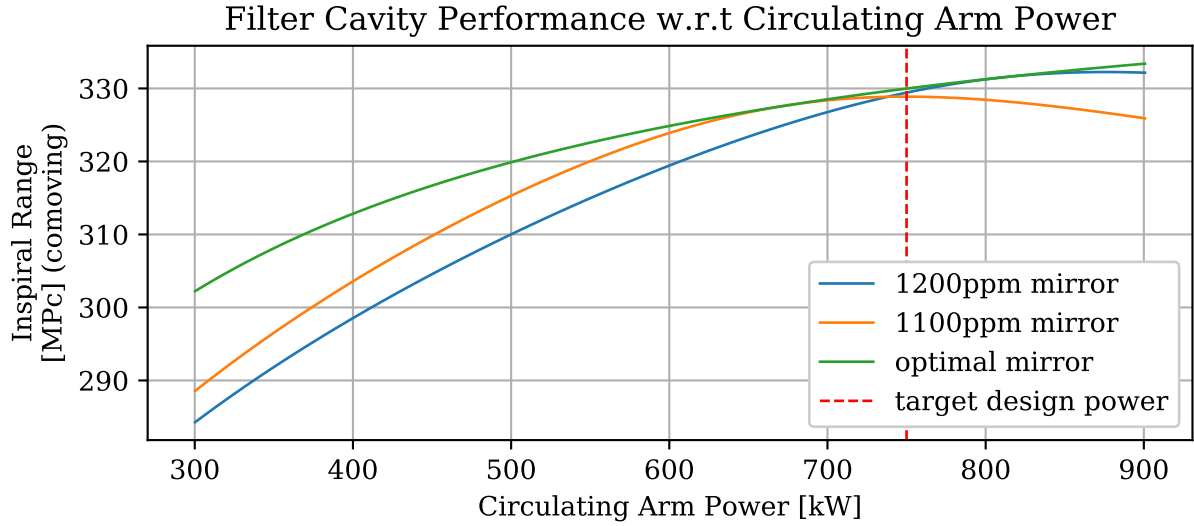


Figure 23: A+ inspiral range as function of the IFO circulating power for different transmissions of the **FC** input coupler.

The conclusion from Figs. 23 and 24 is that the optimal T_{in} to maximize the A+ range indeed changes as function of the circulating power, as expected given that f_{SQL} changes with the power. At the target operating power of 800 kW both $T_{in}=1200\text{ppm}$ and $T_{in}=1100\text{ppm}$ are nearly optimal, while $T_{in}=1200\text{ppm}$ gives about 10 Mpc less than $T_{in}=1100\text{ppm}$ for lower power, while the opposite is true for higher power. Both choices, or values in between, are therefore acceptable, with lower T_{in} to be preferred, as it is unlikely that A+ will ever operate at higher power than 800 kW.

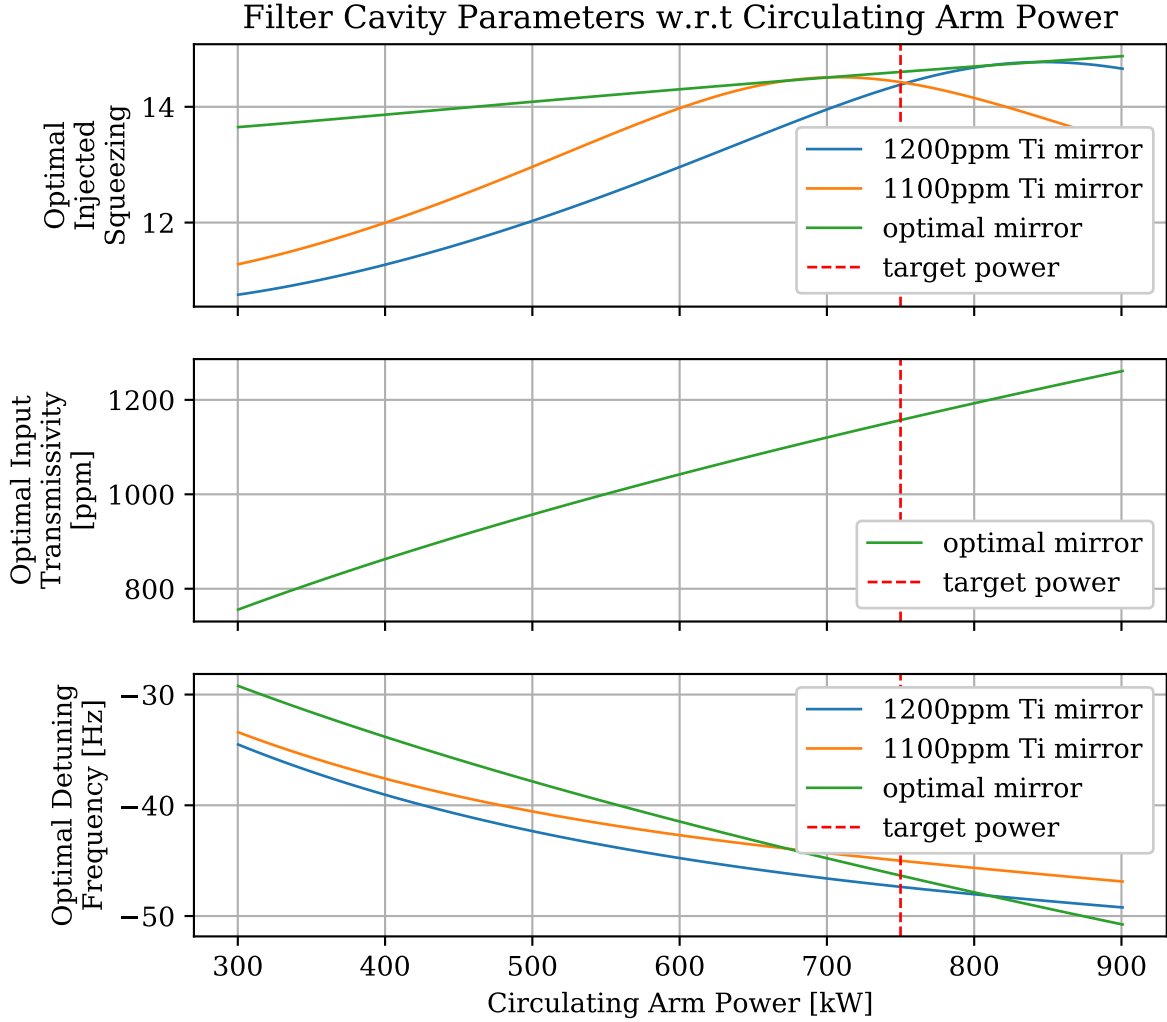


Figure 24: Companion figure of Fig. 23, showing how the optimal level of injected squeezing and optimal detuning frequency change as function of the IFO circulating power for different transmissions of the [FC](#) input coupler.

A.3 Coating Thermal Noise Dependence

The A+ target sensitivity assumes a factor of 2 reduction in coating thermal noise (CTN) over Advanced LIGO. Fig. 25 answers the question of how sub-optimal would the A+ design [FC](#) parameters, in case the A+ CTN is either higher or lower with respect to the A+ target CTN.

Several curves are shown: the blue one represents the baseline A+ [FC](#) where the squeezing level and detuning are optimized, but the mirror is fixed.

The dashed and dotted curves show additional optimizations of the mirrors which would require altering hardware, such as the [FC](#) mirror transmissivity or of SRM transmission and SRC detuning. The conclusion from this plot is that the proposed [FC](#) parameters are nearly optimal and that lack of improvement to CTN can not be compensated with SRC detuning. A 100m scale [FC](#) is also represented. As expected, if the CTN is at the Advanced LIGO

level, a 100m FC is nearly equivalent to a 300m one, while the 300m FC provides 10% higher range for the nominal A+ CTN level, and increasingly higher benefit as the CTN is further reduced.

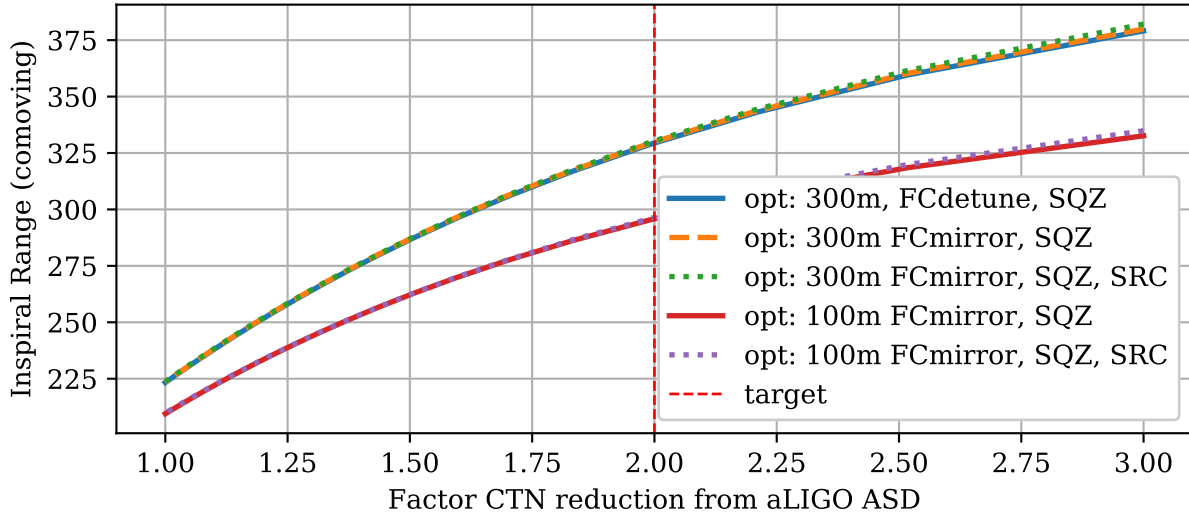


Figure 25: A+ inspiral range as function of the improvement on CTN with respect to the nominal Advanced LIGO CTN. The multiple curves show optimizations of operational parameters such as squeezing level and cavity detuning as well as also hardware parameters such as FC and SRC mirror transmissivity. The current design is optimal at any coating thermal noise.

B Formulas, derivations, references

This section provides some of the details of the calculations presented in this document. Tab. 3 shows a description of the parameters used. Table 4 gives the baseline parameters for the photon sensitivity, filter cavity, and safety margins used in this document.

$\lambda = 1064[\text{nm}]$	Wavelength
$E_\lambda = 1.869 \cdot 10^{-19} [\text{J}]$	Energy of a photon
$Q_\lambda = \sqrt{\frac{E_\lambda}{2}} = 3.05 \cdot 10^{-10} \left[\frac{\sqrt{\text{W}}}{\sqrt{\text{Hz}}} \right]$	ASD of quantum noise as measured by amp. or phase quadratures
$f_{\text{SQL}} = 70[\text{Hz}]$	Frequency of optomechanical ampl. to phase coupling $\mathcal{K}(F) = 1$ at A+ design power
$f_{\text{FC}} = \frac{f_{\text{SQL}}}{\sqrt{2}} = 49.5[\text{Hz}]$	Filter Cavity pole for ideal rotation
$C_{\text{safe}} = 1/10$	ASD safety margin of 10x
$C_{\text{sqz}} = 1/2$	ASD reduction from squeezing (6db observed)

Table 4: Parameters for Filter Cavity Calculations

f_{carrier}	1064 Carrier Frequency [Hz]
\mathcal{F}	cavity Finesse [unitless]
f_Ω	Readout Frequency [Hz]
f_p	Cavity Pole [Hz]
f_{FSR}	Cavity Free Spectral Range [Hz]
f_{det}	Cavity Frequency Detuning [Hz]
ΔL	Cavity length detuning (as endmirror displacement) [m]
λ	wavelength [m]
e_{in}	Field Strength incident on cavity $\sqrt{[W]}$
e_{refl}	Field Strength reflected by cavity $\sqrt{[W]}$
e_{circ}	Field Strength circulating in cavity $\sqrt{[W]}$
r_1, t_1	Input mirror field reflectivity and transmissivity
r_2, t_2	Output mirror field reflectivity and transmissivity
L_{rt}	Cavity round-trip power loss
r_{rt}	Round trip cavity reflectivity (incl. r_1, r_2, L_{rt})

Table 3: Parameters used in the calculations presented in this document.

B.1 Length Sensitivities

B.1.1 Length Sensitivity of a mirror

$$\delta_{\Delta L}^{e_{\text{mirror}}} = \frac{4\pi i}{\lambda} e_{\text{in}} \quad (70)$$

B.1.2 Length sensitivity, Finesse of a Fabry-Perot cavity

Starting with the typical relations for Fabry-Perot cavities:

$$e_{\text{refl}} = r_1 - \frac{t_1^2 \frac{r_{\text{rt}}}{r_1} e^{(2\pi i \frac{2\Delta L}{\lambda})}}{1 - r_{\text{rt}} e^{(2\pi i \frac{2\Delta L}{\lambda})}} e_{\text{in}} = r_1 - \frac{t_1^2 \frac{r_{\text{rt}}}{r_1} e^{(2\pi i \frac{f_{\text{det}}}{f_{\text{FSR}}})}}{1 - r_{\text{rt}} e^{(2\pi i \frac{f_{\text{det}}}{f_{\text{FSR}}})}} e_{\text{in}} \quad (71)$$

$$e_{\text{circ}} = \frac{t_1}{1 - r_{\text{rt}} e^{(2\pi i \frac{f_{\text{det}}}{f_{\text{FSR}}})}} e_{\text{in}} \quad (72)$$

we can derive the phase sensitivity for a Fabry-Perot cavity as:

$$\delta_{\Delta L}^{e_{\text{refl}}} = \left. \frac{de_{\text{refl}}}{d\Delta L} \right|_{\Delta L=0} \quad (73)$$

$$= \frac{r_{\text{rt}}}{r_1} \left(\frac{1 - r_1^2}{(1 - r_{\text{rt}})^2} - \frac{1 - r_1^2}{(1 - r_{\text{rt}})} \right) \frac{4\pi i}{\lambda} e_{\text{in}} \quad (74)$$

Expressions for the cavity pole f_p and the Finesse, \mathcal{F} can also be derived from these, giving:

$$\mathcal{F} = \frac{f_{\text{FSR}}}{2f_p} = \frac{\pi r_{\text{rt}}}{1 - r_{\text{rt}}} \quad (75)$$

$$f_p = \frac{(1 - r_{\text{rt}})f_{\text{FSR}}}{2\pi r_{\text{rt}}} \quad (76)$$

B.1.3 Length Sensitivity, Finesse of Perfectly overcoupled FP Cavity

For a perfectly overcoupled, high-Finesse cavity, we can simplify the above expressions by considering

$$r_{\text{rt}} = r_1 \quad (77)$$

$$T_1 = t_1^2 \text{ small} \quad (78)$$

$$\text{giving} \quad (79)$$

$$r_{\text{rt}} = \sqrt{1 - T_1} \approx 1 - \frac{T_1}{2} \quad (80)$$

so as to obtain:

$$\mathcal{F}_{\text{OC}} = \frac{2\pi}{T_1} = \frac{c}{4L_{\text{FC}}f_p} \quad (81)$$

$$\delta_{\Delta L}^{e_{\text{refl}}} \approx \frac{16\pi i}{T_1\lambda} e_{\text{in}} \approx \frac{i8\mathcal{F}_{\text{OC}}}{\lambda} e_{\text{in}} \approx \frac{i2c}{\lambda f_p L_{\text{FC}}} e_{\text{in}} \quad (82)$$

These final expressions are particularly useful to calculate noise requirements for the A+ (overcoupled) FC.

B.1.4 Detuned Cavity sensitivity

The field generated from cavity length motion with a detuned cavity may be calculated from the on-resonance DC sensitivity above by expressing the quadratures generated by the field modulation, split into the upper and lower sidebands, as well as adding the effect of the detuned cavity transfer function.

$$\mathbf{A} = \frac{1}{\sqrt{2}} \begin{bmatrix} 1 & 1 \\ i & -i \end{bmatrix} \quad (83)$$

$$\vec{H}_{FC\Delta L} = \mathbf{A} \begin{bmatrix} H_{\text{pole}}(f_{\text{carrier}} + f_{\text{det}} + f_{\Omega}) H_{\text{pole}}(f_{\text{carrier}} + f_{\text{det}}) \frac{1}{\sqrt{2}} \delta_{\Delta L}^{e_{\text{refl}}} \\ H_{\text{pole}}^*(f_{\text{carrier}} + f_{\text{det}} - f_{\Omega}) H_{\text{pole}}^*(f_{\text{carrier}} + f_{\text{det}}) \frac{1}{\sqrt{2}} \bar{\delta}_{\Delta L}^{e_{\text{refl}}} \end{bmatrix} \quad (84)$$

Where H_{pole} Is the single pole response of the cavity with the cavity pole f_p , centered around f_{carrier} and normalized to a maximum of 1 since the δ sensitivity is already factored out.

$$H_{\text{pole}}(F) = \frac{if_p}{f_{\text{carrier}} + if_p - F} \quad (85)$$

$$(86)$$

The length sensitivity of the detuned cavity across arbitrary quadratures is

$$|\vec{H}_{FC\Delta L}(f_{\Omega})| = \left(|H_{\text{pole}}(f_{\text{carrier}} + f_{\text{det}} + f_{\Omega})|^2 \right. \quad (87)$$

$$\left. + |H_{\text{pole}}^*(f_{\text{carrier}} + f_{\text{det}} - f_{\Omega})|^2 \right)^{1/2} |H_{\text{pole}}(f_{\text{carrier}} + f_{\text{det}})| \delta_{\Delta L}^{e_{\text{refl}}} \quad (88)$$

where the RHS is due to \mathbf{A} being unitary in the above definition.

$$|\vec{H}_{FC\Delta L}(f_{\Omega})| = \left(\frac{(f_{\text{det}} + f_{\Omega})^2}{2f_p^2} + \frac{(f_{\text{det}} - f_{\Omega})^2}{2f_p^2} + 1 \right)^{-1/2} \left(\frac{f_{\text{det}}^2}{f_p^2} + 1 \right)^{-1/2} \delta_{\Delta L}^{e_{\text{refl}}} \quad (89)$$

C Suspension and seismic models

C.1 HAM ISI

To generate the backscatter noise limit plots, as well as the drive noise for the controls feasibility, we used data and models for the ISI and Suspension models. The ISI data comes from [T1800066](#), although it is regenerated from the SEISvn code, to use different suspension point projections, as well as to better account for “typical” translation noise (shown here larger than in the reference, and closer to the pitch noise). Fig. 26 shows the spectra from this dataset. The data does not include cross spectra, so that aspect cannot be included in the models.

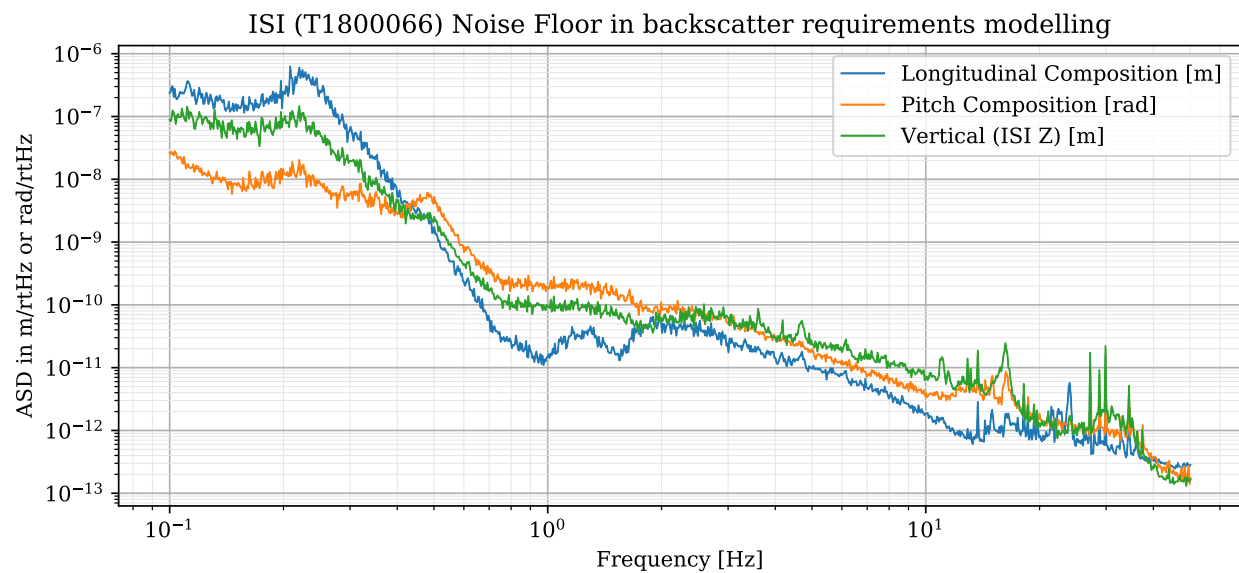


Figure 26: ISI Longitudinal, Pitch and vertical noises from [T1800066](#), recalculated to separate constituent motions from the documents [HSTS](#) suspension point motion. The noise limits of this document use these spectra also for roll and transverse noise

C.2 HSTS (Small Triple Suspension)

The [HSTS](#) noise propagation uses the state-space model from the sus-SVN. This model has been augmented slightly to raise the ground (ISI) suspension point to couple some pitch into longitude. The \mathbb{B} matrix was adjusted to put a 1-meter coupling of the ground-pitch input into the same state D.O.Fs as the ground-longitude input.

The state spaces transfer functions are then attached to the spectra of the ISI above. The state space models have very limited cross coupling, only showing the pitch/longitude couplings, but with no ability to parameterize other couplings. These models are also generated with an OSEM loop built-in. The OSEM noise used is $1\text{e-}10 \frac{\text{m}}{\sqrt{\text{Hz}}}$ at 1Hz, falling as $f^{-1/2}$ (flicker noise of the OSEM LEDs). This number is taken from T0900496. Since the OSEM loop is poorly designed in the state space, the noise is taken to drop with an additional f^{-2} at 10Hz, mimicking the rolloff used in real loops.

Figures 28 and 29 show the transfer functions generated by this state-space export.

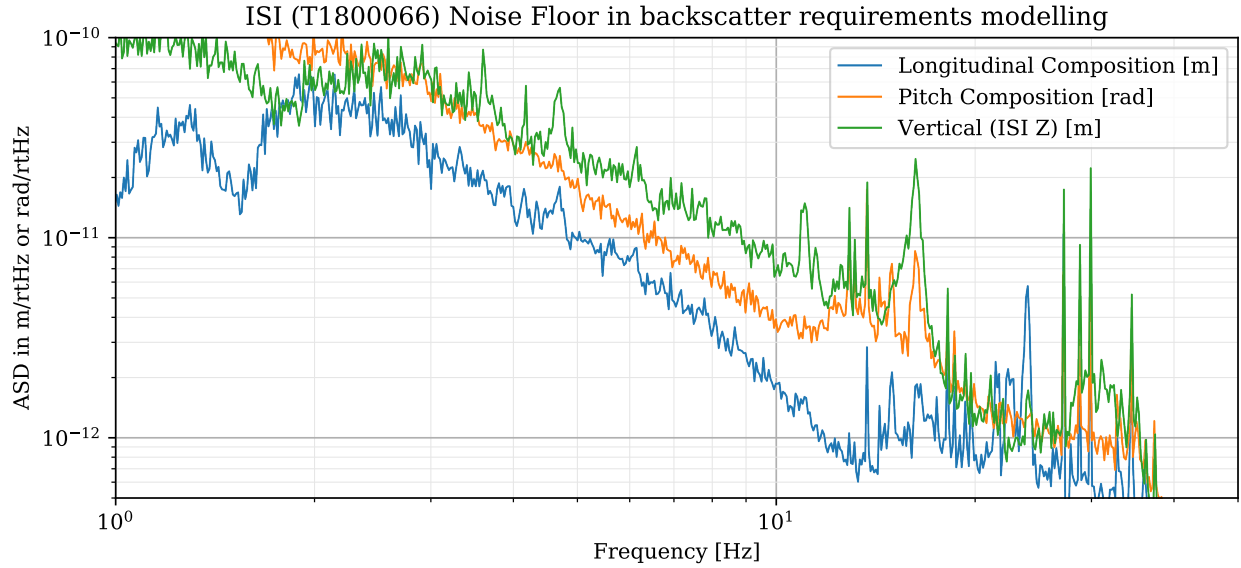


Figure 27: Zoomed version of Fig. 26. This shows an increase in longitudinal noise compared to Fig 9 of T1800066 as it uses the maximum ASD of the 4 datasets, unlike that figure.

C.3 HTTS (Tip-Tilt Suspension)

Like the small triple suspension, the tip tilt model from the sus SVN was used. It was also augmented slightly to include the ground offset from the ISI.

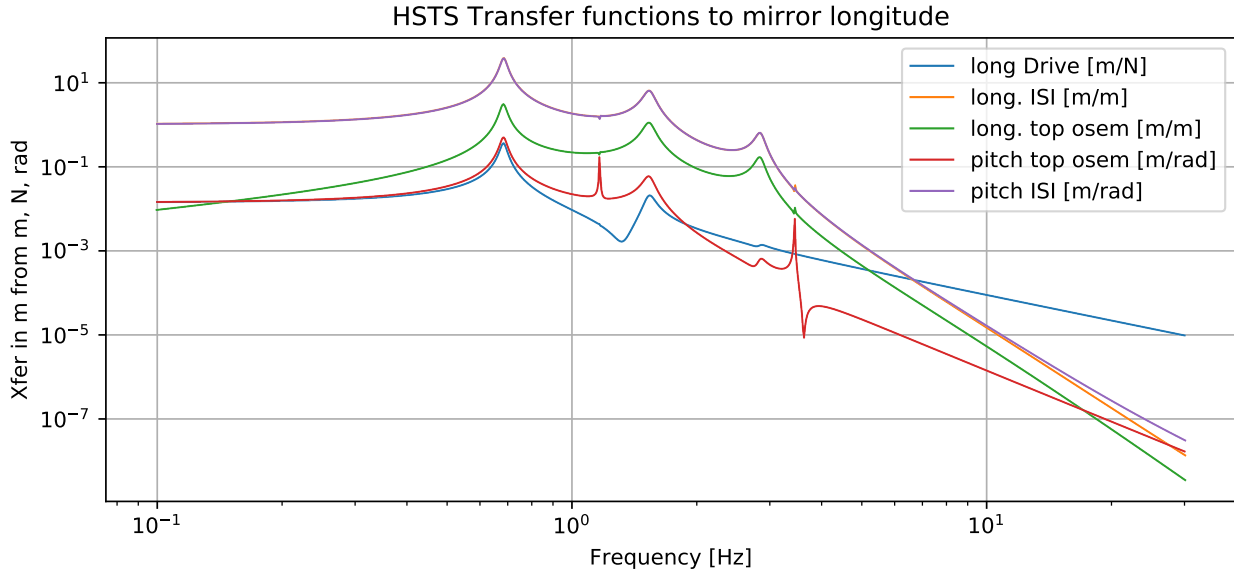


Figure 28: HSTS transfer functions to mirror longitudinal motion.

C.4 Suspension point height for P2L

The state-space models used here are modeled where the ground coupling is actually referring to the topmost attachment of the pendulum wires to the ground. For realistic noise models, either the ISI noise must be referred to this point, or the suspension model must be modified to represent the true ground point. With an estimate of the suspension height, the latter method is used for these noise limits. The **B** input coupling matrix is modified to add some of the “longitude” [Degree of Freedom \(DOF\)](#) to the input “pitch” [DOF](#) column, scaled by the height. The same thing is done to couple ISI roll into the transverse states.

This is important to model well, since the pitch motion of the ISI’s is currently the dominant contributor to longitudinal noise in 1m suspensions. This is indicated in Fig 9. of T1800066; however, looking back through the data from this document (it is in the SeiSVN) shows that this plot could be regenerated taking the worst-case of the 3 LLO and 1 LHO timeperiods used to get the motion shown if Figures 26 and 27. These figures show that the pitch noise is dominant for suspension points taller than 0.5m above the ISI reference frame.

The code for the state-space adjustment looks like (in python):

```

height_m = 1
#This adjustment raises the suspension point
#from being the ISI to 1m over the ISI
idx_P = self.names_in.index('pitch_gnd')
idx_L = self.names_in.index('long_gnd')
idx_R = self.names_in.index('roll_gnd')
idx_T = self.names_in.index('transverse_gnd')
B[:, idx_P] = B[:, idx_P] + height_m * B[:, idx_L]
B[:, idx_R] = B[:, idx_R] + height_m * B[:, idx_T]
```

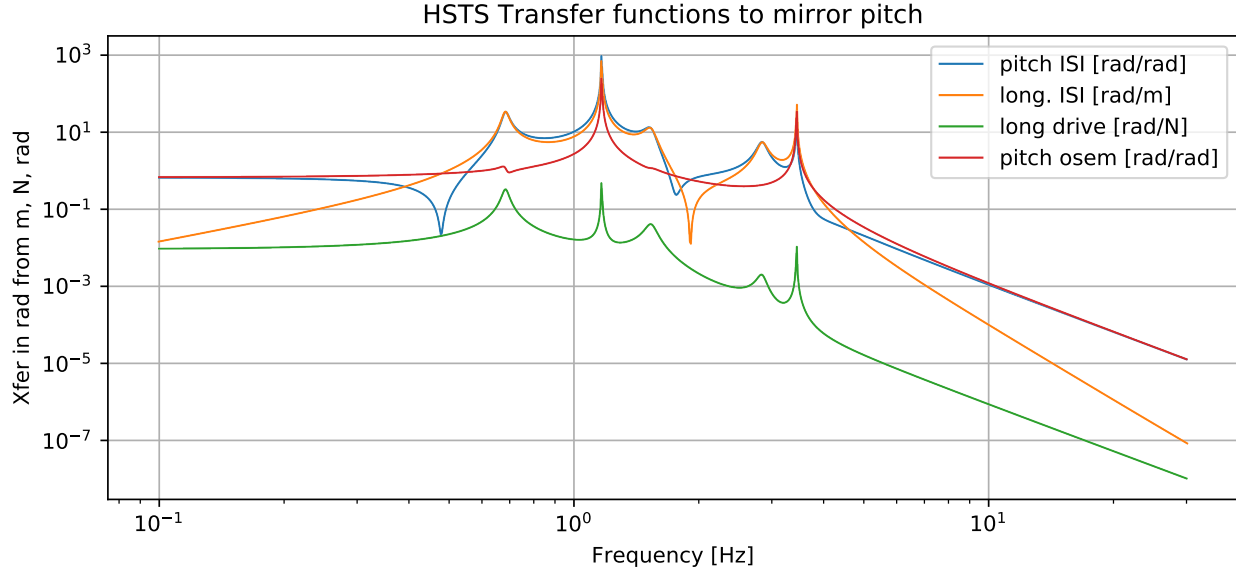


Figure 29: HSTS transfer functions to mirror pitch.

SUS	Height
HSTS	1m
HTTS	0.3m
OPOS	0.3m
OMCS	0.3m

Table 5: Suspension point heights used for noise projections

D Details of FC length control loop

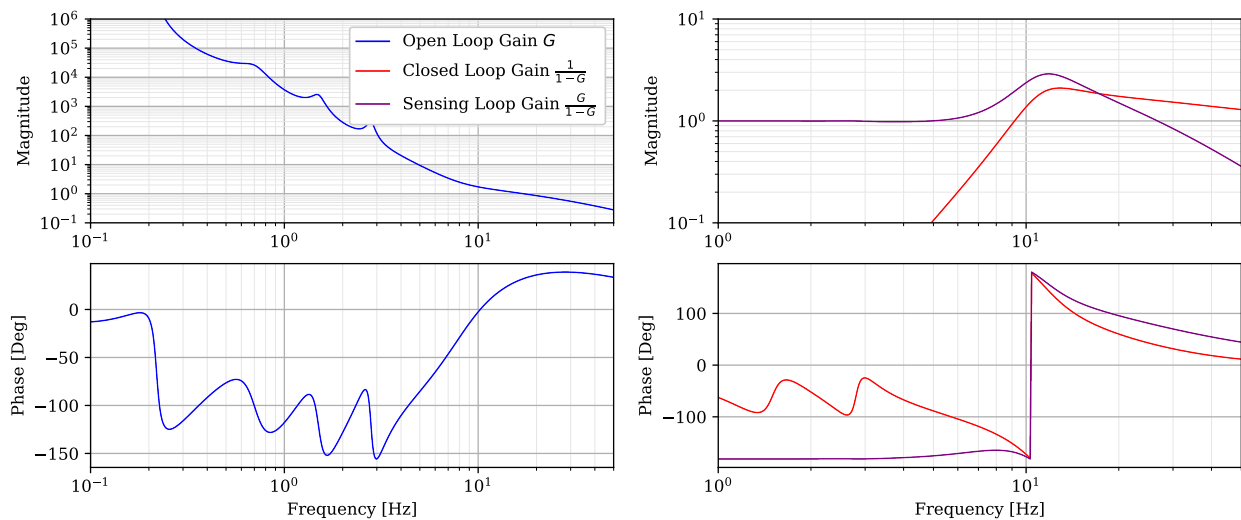
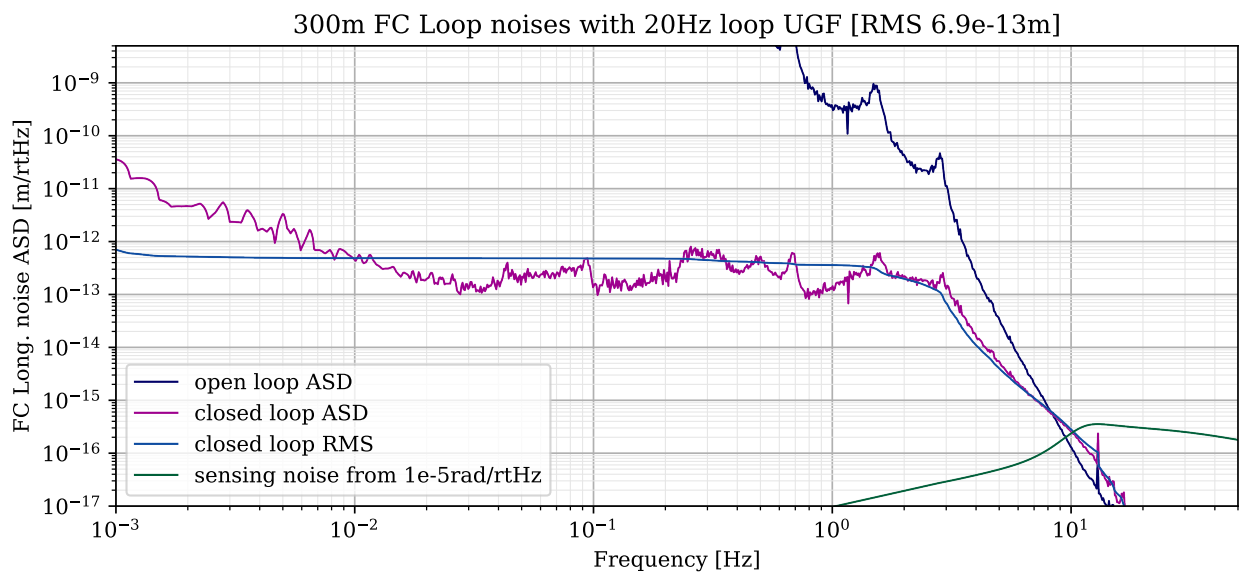
D.1 Length control loop with 20Hz UGF

This section summarizes the details of the control loop of the FC length with 20Hz UGF. Tab. 6 lists the pole and zeros of the controller, Fig. 30 shows the open loop and closed loop transfer functions, while Fig. ?? shows the amplitude spectrum of the residual FC length noise, as well as its RMS.

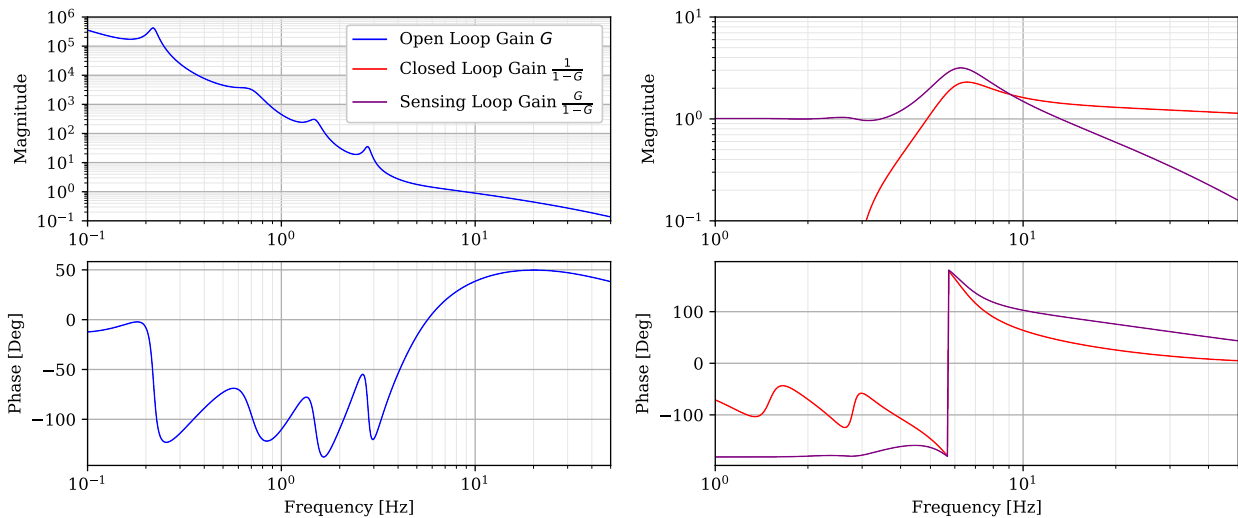
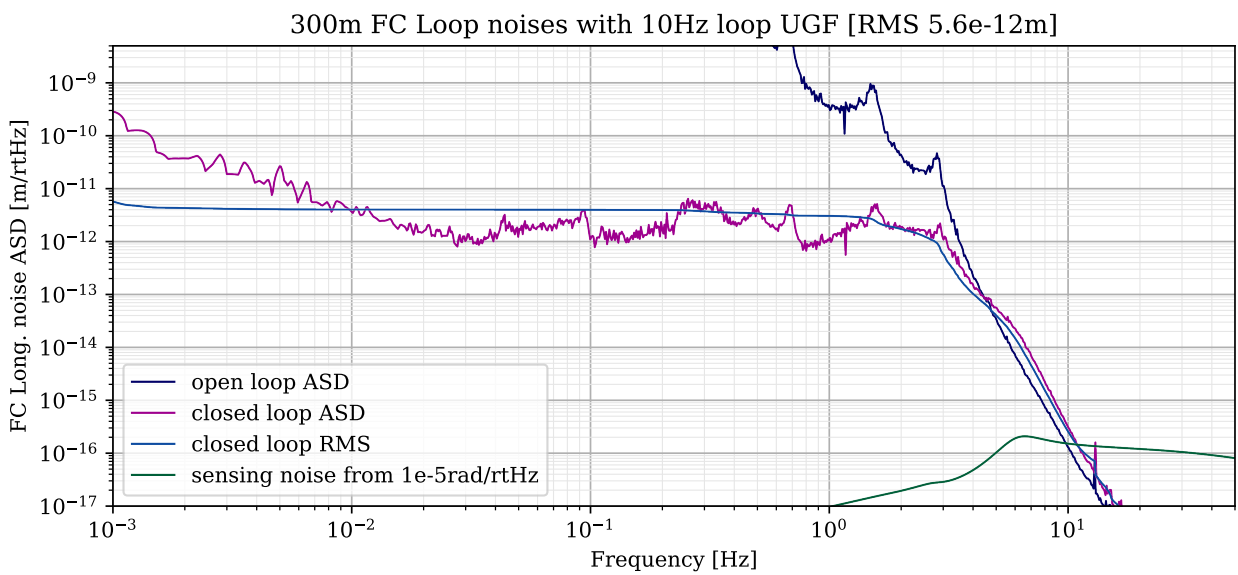
D.1.1 Length control loop with 10Hz UGF

This section summarizes the details of the control loop of the FC length with 10Hz UGF. Tab. 7 lists the pole and zeros of the controller, Fig. 32 shows the open loop and closed loop transfer functions, while Fig. 33 shows the amplitude spectrum of the residual FC length noise, as well as its RMS.

zeros [Hz]	poles [Hz]	Reasoning
	-.1	$1/f$
	-50	rolloff
$-4 \pm 7i$	0, 0	$1/f^2$ boost with weak antiboost near UGF
$-.15 \pm 0.22j$	$-.01 \pm 0.22j$	resgain for HSTS
$-.5 \pm 2.8j$	$-.1 \pm 2.8j$	resgain for HSTS
$-.5 \pm 1.5j$	$-.1 \pm 1.5j$	resgain for HSTS
$-.5 \pm 0.7j$	$-.1 \pm 0.7j$	resgain for HSTS

Table 6: Details of the FC length control loop to obtain a 20Hz UGF.**Figure 30:** Transfer functions of the FC length control loop tuned for a 20 Hz UGF.**Figure 31:** FC length noise and RMS with a 20Hz control loop.

zeros [Hz]	poles [Hz]	Reasoning
	-.1	$1/f$
	-50	rolloff
$-2 \pm 3.5i$	0, 0	$1/f^2$ boost with weak antiboost near UGF
$-.15 \pm 0.22j$	$-.01 \pm 0.22j$	resgain for HSTS
$-.5 \pm 2.8j$	$-.1 \pm 2.8j$	resgain for HSTS
$-.5 \pm 1.5j$	$-.1 \pm 1.5j$	resgain for HSTS
$-.5 \pm 0.7j$	$-.1 \pm 0.7j$	resgain for HSTS

Table 7: Details of the FC length control loop to obtain a 10Hz UGF.**Figure 32:** Transfer functions of the FC length control loop tuned for a 10 Hz UGF.**Figure 33:** FC length noise and RMS with a 10Hz control loop.

E RLF phase noise derivations

E.1 Length Noise Requirement

There is approx 20mW of light from the IFO for frige-offset DC readout.

$$P_{\text{AS}} = 20\text{mW} \quad (90)$$

We are designing for 90 DB of total isolation of this light to the filter cavity by including 3 Faraday Isolators.

$$P_{\text{sc}} = 10^{-90/10} P_{\text{AS}} = 20\text{pW} \quad (91)$$

The optical gain of the cavity depends on its length and bandwidth, and it enhances both the carrier and sidebands, giving a modulation gain

$$p_{\text{sb}} = \frac{4\pi}{\lambda} \frac{c}{2\gamma L} \sqrt{P_{\text{sc}}} x \quad (92)$$

Where λ is the laser wavelength, and L is the cavity length. The factor of 2 in the denominator is from the cavity being detuned, which lowers the gain at low frequencies by $\sqrt{2}$ for both the carrier and the sidebands.

For the chosen FC1 mirror transmissivity of 0.001, which is optimal for $\sim 400\text{kW}$ arm power in LIGO (using the current SRM transmissivity), the cavity pole is:

$$\gamma \approx 2\pi \cdot 40\text{Hz} \quad (93)$$

This leads to a quantum noise limited length sensitivity for the cavity, from the backscattered light, of

$$\Delta L^2 = \left(\frac{\partial p_{\text{sb}}}{\partial x} \right)^{-2} \frac{\hbar\omega}{2} \quad \omega = \frac{2\pi c}{\lambda} \quad (94)$$

calculating this gives the break even point where filter cavity noise will show equal to DARM quantum noise. DARM quantum noise includes the radiation pressure contribution, as the modulated backscatter field can create amplitude modulations which push on the mirrors. This limit so far also does not include the improvement in quantum noise due to frequency-dependent squeezing.

$$\Delta L_{\text{lim}} = 2.9 \cdot 10^{-15} \frac{\text{m}}{\sqrt{\text{Hz}}} \quad (95)$$

If we include both 6db squeezing, and a safety margin of 10 in the amplitude spectral density, then the safe limit is:

$$\Delta L_{\text{safe}} = 1.4 \cdot 10^{-16} \frac{\text{m}}{\sqrt{\text{Hz}}} \quad (96)$$

E.2 Sensing injected length noise

With the length noise established, we must consider the frequency stability required for sensing field to achieve that length noise sensitivity, and we must determine how this “witness” noise is injected as real noise through a feedback control system.

The frequency noise of any sensing field is related to the witness length noise of the cavity through

$$\frac{\Delta L}{L} = \frac{\Delta F}{F} \quad \text{with } F = \frac{\omega}{2\pi} = 282\text{THz} \quad (97)$$

Using the safe limit for length noise, this gives

$$\Delta F_{\text{safe}}^* = 136 \frac{\mu\text{Hz}}{\sqrt{\text{Hz}}} \quad (98)$$

The star indicates that it is not yet a limit, as we must account for the control system performance. Already though, it is apparent that typical laser stabilization with a reference cavity will struggle to achieve this performance, as those typically only reach mHz/ $\sqrt{\text{Hz}}$ levels.

To relate this to the control system, we must determine how much of this witness length noise is injected into the cavity. For a control open loop gain $G(f)$. This effective length noise becomes a real noise through the closed loop response $\bar{G}(f)$.

$$\bar{G}(f) = \frac{G(f)}{1 - G(f)} \quad (99)$$

The true safe length noise, accounting for the loop, is:

$$\Delta F_{\text{safe}} = |\bar{G}(f)|^{-1} \Delta F_{\text{safe}}^* \quad (100)$$

for simplicity, we can analyze implication of this limit by choosing a simple 1/f loop with a unity gain frequency f_{ugf} . This gives:

$$G(f) = i \frac{f_{\text{ugf}}}{f} \quad \bar{G}(f) = \frac{f_{\text{ugf}}}{f_{\text{ugf}} + if} \quad (101)$$

and in particular,

$$|\bar{G}(f)|^{-1} \approx \frac{f}{f_{\text{ugf}}} \quad (102)$$

E.3 Phase noise requirement

Finally, phase noise related to frequency noise as they are both fundamentally the same physical modulations on the laser light, related by

$$\Delta\phi = \frac{\Delta F(f)}{f} \quad (103)$$

Using the approximations for the closed loop sensing gain of eq. 102, the phase noise requirement is related to the UGF by:

$$\Delta\phi = |\bar{G}(f)|^{-1} \frac{\Delta F(f)}{f} \approx \frac{\Delta F(f)}{f_{\text{ugf}}} \quad (104)$$

for a 10Hz ugf, which is essentially as low as the HSTS + HAM isi can go and still keep reasonable FC length noise, the phase noise requirement ends up as:

$$\Delta\phi_{\text{safe}} = 1.36 \cdot 10^{-5} \frac{\text{Rad}}{\sqrt{\text{Hz}}} \quad (105)$$

One can then consider the length noise requirement to maintain this phase noise and it is simply unreasonable. Furthermore, this is a challenge even ignoring the squeezing and safety factors. In fact, the only light source available with this absolute stability is the interferometer itself. Furthermore, the phase noise budget for the existing fiber delivery system cannot preserve this phase noise in a sensing field, even if it could be made. See figure Fig. 34.

This issue is a considerable one, so it is worth noting how it may be relaxed. Because of additional freedom in designing the control loop, the safe limit of eq. 105 is only representative for frequencies between a factor of 3-6 above the length feedback loop unity gain frequency, above which the loop rolloff can dominate and the limit is relaxed.

E.4 Condensed Expressions

These expressions combine the above analysis into a single expression to determine the allowable phase and frequency noise. They do not include the safety and squeezing improvement factors.

$$\Delta F(f) = \bar{G}(f) \frac{\gamma}{2\pi} \sqrt{\frac{\hbar\omega}{2P_{\text{sc}}}} \quad (106)$$

$$\Delta\phi(f) = \frac{\bar{G}(f)}{f} \frac{\gamma}{2\pi} \sqrt{\frac{\hbar\omega}{2P_{\text{sc}}}} \approx \frac{1}{f_{\text{ugf}}} \frac{\gamma}{2\pi} \sqrt{\frac{\hbar\omega}{2P_{\text{sc}}}} \quad (107)$$

The important thing to note in these expressions is that the required phase noise to sense the cavity is essentially the same as the phase noise allowable for relay optics which carry

the backscatter, only relaxed by the ratio of the unity-gain-frequency to the cavity pole. The experimental consequence is that any resonant length-sensing light supplied from an external source must be as stable as the backscatter itself. This requires active stabilization with the phase sensing entirely within the vacuum chamber. The RLF scheme achieves this through stability inheritance of the CLF feedback with the interferometer as the local oscillator.

E.5 Phase Noise Measurements

This section just includes a plot of the phase noise measured in the LLO LIGO squeezing system loops ([LLO44475](#)).

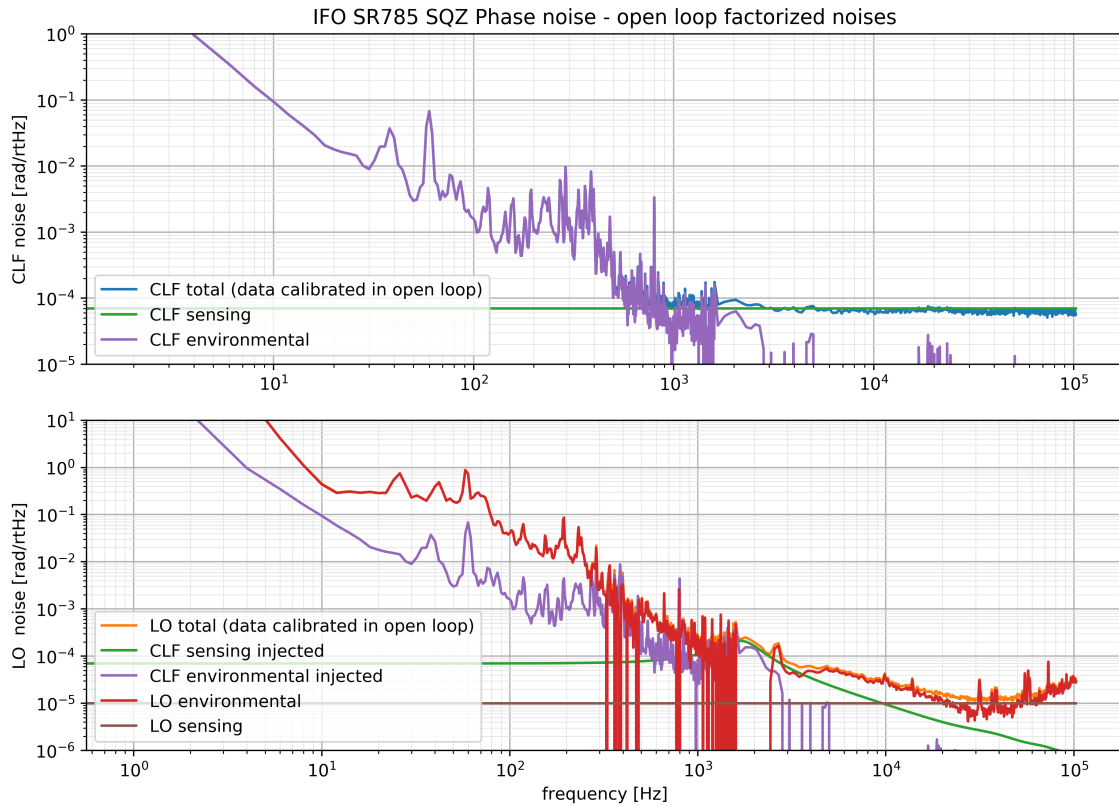


Figure 34: Open Loop phase noise in the squeezing system. The curves labeled environmental include both the acoustic pickup and fiber delivery noise on the squeezer sensing fields (from pump and CLF light). The CLF spectrum includes shorter fibers, but also the 200MHz VCO oscillator noise. The LO spectrum primarily includes the phase noise from the long fiber delivering light from the PSL.

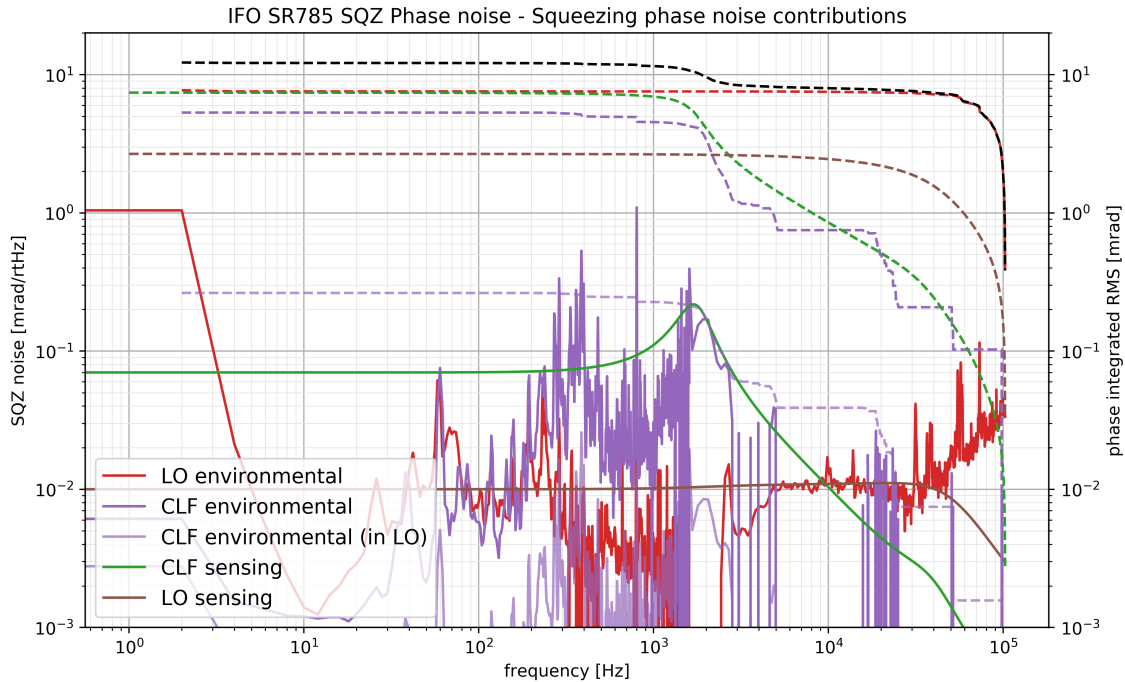


Figure 35: Closed Loop phase noise in the squeezing system. This represents the residual noise of the CLF that is injected into the RLF, in addition to the sensing noise that is injected. This shows that the loop gain sufficiently suppresses external noises, and the RLF phase noise will be dominated by the sensing noise level.

Acronyms

AWC Active wavefront control.

BHD Balanced Homodyne Readout.

CLF Coherent Locking Field.

CTN Coating Thermal Noise.

DCPD DC photo-diodes used for interferometer readout.

DOF Degree of Freedom.

FC Filter cavity.

FSR Free Spectral Range.

HSTS Small triple suspension.

HTTS Tip-tilt suspension.

IFO Interferometer.

OFI Output Faraday Isolator.

OFIS Output Faraday Isolator Suspension.

OMC Output Mode Cleaner.

OPO Optical Parametric Oscillator.

OPOS OPO Suspension.

RPN Radiation Pressure Noise.

References

- [1] P. Kwee, J. Miller, T. Isogai, L. Barsotti, and M. Evans, *Decoherence and degradation of squeezed states in quantum filter cavities*, [PhysRevD.90.062006](#)
- [2] H. J. Kimble, Yuri Levin, Andrey B. Matsko, Kip S. Thorne, and Sergey P. Vyatchanin, *Conversion of conventional gravitational-wave interferometers into quantum nondemolition interferometers by modifying their input and/or output optics*, [PhysRevD.65.022002](#)
- [3] T. Isogai, J. Miller, P. Kwee, L. Barsotti, and M. Evans, *Loss in long-storage-time optical cavities*, [Optics Express Vol. 21, Issue 24, pp. 30114-30125 \(2013\)](#)
- [4] M. Evans, L. Barsotti, P. Kwee, J. Harms, and H. Miao, *Realistic filter cavities for advanced gravitational wave detectors*, [PhysRevD.88.022002](#)
- [5] E. Oelker et al, *Audio-Band Frequency-Dependent Squeezing for Gravitational-Wave Detectors* [PhysRevLett.116.041102](#)